TU Delft

Delft University of Technology

Document Version
Final published version

Licence
Dutch Copyright Act (Article 25fa)

Citation (APA)
Evangelisti, G., Santina, C. D., & Hirche, S. (2026). Exponentially Stable Projector-Based Control of Lagrangian Systems With Gaussian Processes. *IEEE Transactions on Automatic Control*, *71*(7), 4435-4449. https://doi.org/10.1109/TAC.2026.3662545

Important note
To cite this publication, please use the final published version (if applicable).
Please check the document version above.

Copyright
In case the licence states “Dutch Copyright Act (Article 25fa)”, this publication was made available Green Open Access via the TU Delft Institutional Repository pursuant to Dutch Copyright Act (Article 25fa, the Taverne amendment). This provision does not affect copyright ownership.
Unless copyright is transferred by contract or statute, it remains with the copyright holder.

Sharing and reuse
Other than for strictly personal use, it is not permitted to download, forward or distribute the text or part of it, without the consent of the author(s) and/or copyright holder(s), unless the work is under an open content license such as Creative Commons.

Takedown policy
Please contact us and provide details if you believe this document breaches copyrights.
We will remove access to the work immediately and investigate your claim.

This work is downloaded from Delft University of Technology.

Exponentially Stable Projector-Based Control of Lagrangian Systems With Gaussian Processes

Giulio Evangelisti, Cosimo Della Santina, *Senior Member, IEEE*, and Sandra Hirche, *Fellow, IEEE*

***Abstract*—Designing accurate yet reliable tracking controllers with tight performance guarantees for Lagrangian systems is challenging due to nonlinear modeling uncertainties and conservative stability criteria. This article proposes a structure-preserving projector-based tracking control law for uncertain Euler–Lagrange systems using physically consistent Lagrangian–Gaussian processes (L-GPs). We leverage the uncertainty quantification of the L-GP for adaptive feedforward-feedback balancing. In particular, an accurate probabilistic guarantee for exponential stability is derived by leveraging matrix analysis results and ideas from contraction analysis, where the benefit of the proposed controller is proven and shown in the closed-form expressions for convergence rate and radius. Extensive numerical simulations not only demonstrate the controller's efficacy based on a two-link and a soft robotic manipulator, but also all theoretical results are explicitly analyzed and validated.**

***Index Terms*—Adaptive control, Gaussian processes (GPs), machine learning, robotics, stability of nonlinear systems.**

I. Introduction

DATA-DRIVEN methods offer a promising approach to enhance the performance, reliability, and safety of traditional control strategies based on parameteric mathematical models. Gaussian processes (GPs) stand out among these methods due to their data-efficiency and uncertainty quantification. However, neither GPs nor other data-driven methods generally account for physical consistency [1], limiting their applicability in model-based control and the accuracy of providable guarantees.

Physics-informed machine learning has been shown to improve the methods' data efficiency and reliability by encoding the variational Euler–Lagrange (EL) structure into data-driven models for mechanical and electromagnetic systems [2], [3], [4], [5]. In particular, deep learning with neural networks has shown auspicious results for robotic systems [6]. However, these methods typically lack a measure for uncertainty quantification, hampering the provision of safety guarantees, such as in, e.g., [7], where deep Lagrangian networks (DeLaNs) and their passivity properties are leveraged for a learning-based implementation of an energy-based controller [8] for under-actuated systems. Here, sufficiently low modeling errors are an inevitable requirement, which can only be satisfied in regions near the training domain.

Applying GPs to learning-based control of robotic systems was initially proposed for local regression in a computed torque control scheme [9], yet without any stability guarantees. When safety is explicitly considered in data-driven control methods, guarantees often critically depend on the prior availability of a known dynamical model based on which, e.g., a reachability analysis for robotic systems with state-dependent disturbances can be performed [10]. Feedback compensation of these residual dynamics based on closed-box modeling with GPs is proposed in [11] for EL systems together with an uncertainty-adaptive computed torque controller. Here, due to multiple applications of Young's inequality, the exponential convergence result suffers from conservatism and dependencies on several positive parameters that are assumed to exist. A GP-based feedback linearizing control law is formulated in [12] but is limited to single-input systems in controllable canonical form while asymptotic stability of the tracking error is only guaranteed in the noiseless case, reducing to ultimate boundedness otherwise. Performances of model predictive controllers have also been shown to improve significantly with learning via GPs [13], where closed-loop stability guarantees have been proven for linear time-invariant systems [14] or input-to-state stability for nonlinear discrete-time systems [15].

In the context of structure-preserving control, several different approaches have been proposed. An optimal control problem with respect to the external torque applied to a single rigid body is analyzed in [16], but potential fields are assumed to be absent, and a numerical solution of optimality conditions up to the fourth order is required. A proportional-derivative controller is naturally generated in [17] by leveraging the inherent impedance of the underlying soft robot. Therefore, its softness is preserved for potential environmental interactions, yet only linear stiffness and damping matrices are considered while gravity is fully compensated. Also contraction-based control design has gained a significant amount of research attention. However, it leads to

Received 26 August 2025; accepted 12 January 2026. Date of publication 9 February 2026; date of current version 1 July 2026. This work was supported in part by the Consolidator Grant "Safe data-driven control for human-centric systems" (CO-MAN) of the European Research Council (ERC) of the European Union (EU) under Grant 864686, and in part by the Konrad Zuse School of Excellence in reliable AI (relAI). Recommended by Associate Editor F. Pasqualetti. *(Corresponding author: Giulio Evangelisti.)*

Giulio Evangelisti and Sandra Hirche are with the Chair of Information-oriented Control, TUM School of Computation, Information and Technology, the Munich Data Science Institute, and the Munich Institute of Robotics and Machine Intelligence, Technical University of Munich, 80333 Munich, Germany (e-mail: g.evangelisti@tum.de; hirche@tum.de).

Cosimo Della Santina is with the Cognitive Robotics Department, Delft University of Technology, 2628 CD Delft, The Netherlands (e-mail: c.dellasantina@tudelft.nl).

Digital Object Identifier 10.1109/TAC.2026.3662545

1558-2523 © 2026 IEEE. All rights reserved, including rights for text and data mining, and training of artificial intelligence and similar technologies. Personal use is permitted, but republication/redistribution requires IEEE permission. See https://www.ieee.org/publications/rights/index.html for more information.

Authorized licensed use limited to: TU Delft Library. Downloaded on July 10,2026 at 10:21:06 UTC from IEEE Xplore. Restrictions apply.

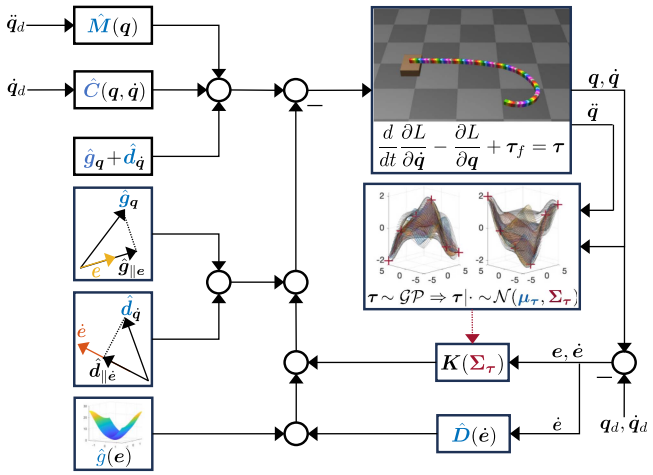


Fig. 1. Block scheme of the proposed projector-based L-GP control with uncertainty-adaptive feedback: $\hat{M}$, $\hat{C}$, $\hat{g}_q$, and $\hat{d}_{\dot{q}}$ denote the learned components (blue), i.e., the inertia, Coriolis matrix, gravity, and friction, respectively, of the system with uncertain Lagrangian L. The covariance estimate Σ_τ (red) is used to adapt the feedback gains.

the so-called integrability problem [18] for nonlinear systems due to the involved Jacobians and, therein, partial derivatives with respect to the controllers. Moreover, trajectory tracking using control contraction metrics [19] is typically based on the analysis of virtual displacements. In contrast, our analysis approach circumvents this necessity by directly exploiting the analytical structure of the considered EL systems. Partial contraction analysis [20] can lead to similar exponential results as ours, but still requires studying contractivity of the auxiliary system via Jacobians. Altogether, leveraging physically consistent methods in learning-based control of robotic systems while being able to provide accurate stability guarantees for high performance and reliability is still an ongoing open problem. This article addresses these issues by leveraging the physical consistency of Lagrangian–Gaussian processes (L-GPs) from [1] in an uncertainty-adaptive control framework combined with rigorous theoretical guarantees.

A. Contribution

We propose a novel structure-preserving control design, which is schematically depicted in Fig. 1, and uses projectors to compensate the system's dynamics only when necessary, while leveraging the L-GP's covariance estimate for confidence-dependent gain adaptation. By preserving the system's dynamical structure, we aim to achieve reliable tracking performance despite remaining model uncertainties. At the same time, we exploit the learned model with projections to make use of the natural potential and dissipative forces driving toward the control goal, i.e., the desired trajectory in the state space. Moreover, a novel exponential stability result is derived based on intermediate matrix analysis results and arguments from contraction theory applied to Lagrangian systems. The integrability problem of contraction theory-based control due to the dependence on Jacobians is circumvented by directly exploiting the dynamics' structure. Analytically compact expressions for time-variant convergence radius and rate are derived with the goal of optimizing the tightness of the resulting bounds. At the same time, these stability results also significantly extend our earlier work, which combines the L-GP [21] with the standard augmented proportional-derivative (PD+) controller [22], the latter is considered de-facto as the state of the art (SoA) in this work. All theoretical contributions are validated in numerical experiments, further underlining the practical efficacy of the proposed methods. Note that the L-GP modeling framework from [1] is applied but does not represent a contribution of the present work.

The rest of this article is organized as follows. After formally introducing our considered problem setting in Section II, we first provide a brief overview of the modeling framework of L-GPs in Section III. The proposed control design is then derived and analyzed in Section IV, followed by validating numerical simulations in Section V. Finally, we summarize our work's theoretical and practical implications in Section VI.

B. Notations

Bold lowercase and uppercase symbols denote vectors $\boldsymbol{a}$ and matrices $\boldsymbol{A}$, respectively, $\bar{a} = \bar{\lambda}(\boldsymbol{A})$ and $\underline{a} = \underline{\lambda}(\boldsymbol{A})$ denote the maximal and minimal eigenvalues of $\boldsymbol{A}$, respectively, $\mathrm{E}[\cdot]$ and $\mathrm{Var}[\cdot]$ denote the expectation and variance operators, respectively, and $\mathbb{R}$ and $\mathbb{N}$ denote the set of real and natural numbers, respectively. $\boldsymbol{I}$ is the identity, $\mathbf{0}$ is the zero, and $\mathbf{1}$ is the ones matrix. $|\cdot|$ indicates the cardinality of a set, $\mathcal{N}(\boldsymbol{\mu}, \boldsymbol{\Sigma})$ denotes a multivariate Gaussian distribution with mean $\boldsymbol{\mu}$ and covariance $\boldsymbol{\Sigma}$, $\|\cdot\|_{\mathcal{L}_2} = \sqrt{\int_0^\infty \|\cdot\|^2 dt}$ denotes the $\mathcal{L}_2$-norm, and $\|\cdot\|$ denotes the Euclidian norm if not stated otherwise. Positive definiteness (respectively, semidefiniteness) of a symmetric matrix is indicated by $\cdot \succ \mathbf{0}$ (respectively, $\cdot \succeq \mathbf{0}$), and $\mathrm{vec}(\cdot)$ stacks the columns of a matrix to form a vector.

II. Problem Formulation

A. Dynamical System

In this article, we focus on uncertain, fully actuated EL systems with equations of motion given by [23]

$$\frac{d}{dt}\frac{\partial L}{\partial \dot{\boldsymbol{q}}} - \frac{\partial L}{\partial \boldsymbol{q}} = \boldsymbol{\tau}_c = \boldsymbol{\tau} - \boldsymbol{\tau}_f \tag{1}$$

with Lagrangian L, generalized coordinates $\boldsymbol{q} \in \mathbb{R}^N$, and generalized forces $\boldsymbol{\tau}_c \in \mathbb{R}^N$. The latter are composed of the difference between the active, possibly underactuated, input $\boldsymbol{\tau}$ and the dissipative friction $\boldsymbol{\tau}_f$. These equations of motion (1) follow according to Hamilton's principle [24] from the stationary solutions of the action integral $I(\boldsymbol{q})$ which, in the homogeneous case for $\boldsymbol{\tau}_c = \mathbf{0}$, is given by $I(\boldsymbol{q}) = \int_{t_1}^{t_2} L(\boldsymbol{q}, \dot{\boldsymbol{q}}) dt$. The inclusion of nonzero generalized forces is done by modifying $I(\boldsymbol{q})$ with so-called Lagrange multipliers, leading to (1).

Assumption 1: The Lagrangian $L \equiv L(\boldsymbol{q}, \dot{\boldsymbol{q}}) = T(\boldsymbol{q}, \dot{\boldsymbol{q}}) - V(\boldsymbol{q})$ in (1) is autonomous and consists of the difference between unknown kinetic energy $T : \mathbb{R}^N \times \mathbb{R}^N \to \mathbb{R}$ and unknown potential energy $V : \mathbb{R}^N \to \mathbb{R}$.

Authorized licensed use limited to: TU Delft Library. Downloaded on July 10,2026 at 10:21:06 UTC from IEEE Xplore. Restrictions apply.

Assumption 2: The kinetic energy is quadratic $T(\boldsymbol{q}, \dot{\boldsymbol{q}}) = \frac{1}{2}\dot{\boldsymbol{q}}^T \boldsymbol{M}(\boldsymbol{q})\dot{\boldsymbol{q}}$ w.r.t. the velocities $\dot{\boldsymbol{q}}$, where $\boldsymbol{M} : \mathbb{R}^N \to \mathbb{R}^{N\times N}$ is the unknown, (symmetric) positive definite, inertia matrix.

Assumption 3: The potential energy is positive-semidefinite and has an equilibrium in the origin, i.e., $V(\boldsymbol{0}) = 0$, $V(\boldsymbol{q}) \geq 0 \forall \boldsymbol{q} \in \mathbb{R}^N$, and $\frac{\partial}{\partial \boldsymbol{q}} V(\boldsymbol{0}) = \boldsymbol{0}$.

Assumption 4: The dissipative friction $\boldsymbol{\tau}_f = \boldsymbol{D}(\dot{\boldsymbol{q}})\dot{\boldsymbol{q}}$ is the matrix-vector product of the generalized velocities with the (symmetric) positive semidefinite damping matrix $\boldsymbol{D}(\dot{\boldsymbol{q}}) \succeq \boldsymbol{0}$.

Assumptions 1–4 describe the considered system class and represent its physical properties. Note that Assumption 1 is nonrestrictive since time-variance and dissipation can be introduced to the conservative left-hand side of (1) via the external force component $\boldsymbol{\tau}_f$. Assumption 2 enforces positivity of the kinetic or electric energy for all nonzeros velocities or currents, respectively, and is valid for, e.g., any nonrelativistic mechanical system, while Assumption 3 requires w.l.o.g. that the chosen coordinates have an equilibrium at the origin. Finally, Assumption 4 assumes a certain friction or resistance structure applicable to various dissipation phenomena, e.g., linear viscous, air-drag, structural, or continuous Coulomb dampings. In case of a purely position- or charge-dependent damping matrix $\boldsymbol{D}(\boldsymbol{q})$, the Rayleigh dissipation potential $R(\boldsymbol{q}, \dot{\boldsymbol{q}}) = \frac{1}{2}\dot{\boldsymbol{q}}^\top \boldsymbol{D}(\boldsymbol{q})\dot{\boldsymbol{q}}$ structurally permits a derivation according to $\boldsymbol{\tau}_f = \frac{\partial R}{\partial \dot{\boldsymbol{q}}} = \boldsymbol{D}(\boldsymbol{q})\dot{\boldsymbol{q}}$.

Remark 1: For conciseness, the remainder of this work focuses on mechanical systems, cf., Assumption 2. However, due to our variational modeling based on generalized energies, the system class (1) naturally includes mechanical, electrical, fluid, thermal [25], and also mixed-nature, e.g., electromechanical [23], systems.

Exploiting Assumptions 1–4 and applying the chain rule to (1), we obtain the well-known matrix-vector expression

$$\boldsymbol{M}(\boldsymbol{q})\ddot{\boldsymbol{q}} + \boldsymbol{C}(\boldsymbol{q}, \dot{\boldsymbol{q}})\dot{\boldsymbol{q}} + \boldsymbol{g}(\boldsymbol{q}) + \boldsymbol{D}(\dot{\boldsymbol{q}})\dot{\boldsymbol{q}} = \boldsymbol{\tau} \tag{2}$$

where $\boldsymbol{M}(\boldsymbol{q}) \in \mathbb{R}^{N\times N}$ is the (symmetric) positive definite, inertia matrix, $\boldsymbol{C}(\boldsymbol{q}, \dot{\boldsymbol{q}}) := \frac{1}{2}\left[\frac{\partial^2 T}{\partial \dot{\boldsymbol{q}} \partial \boldsymbol{q}^\top} + \dot{\boldsymbol{M}}(\boldsymbol{q}) - \frac{\partial^2 T}{\partial \boldsymbol{q} \partial \dot{\boldsymbol{q}}^\top}\right]$ is the generalized Coriolis matrix such that $\dot{\boldsymbol{M}} - 2\boldsymbol{C}$ is skew-symmetric, and $\boldsymbol{g}(\boldsymbol{q}) := \frac{\partial}{\partial \boldsymbol{q}} V$ is the vector of generalized potential forces derived from the potential energy $V(\boldsymbol{q}) \in \mathbb{R}$.

B. Problem Statement

Having specified our considered class of EL systems, we now describe the problem setting.

Objective 1: The overarching goal of this article is to design a learning-based tracking controller for (2) in the form

$$\boldsymbol{\tau} = \boldsymbol{u}(\boldsymbol{q}_d, \dot{\boldsymbol{q}}_d, \ddot{\boldsymbol{q}}_d, \boldsymbol{e}, \dot{\boldsymbol{e}}) - \boldsymbol{K}_P(\boldsymbol{\Sigma}_{\boldsymbol{\tau}})\boldsymbol{e} - \boldsymbol{K}_D(\boldsymbol{\Sigma}_{\boldsymbol{\tau}})\dot{\boldsymbol{e}} \tag{3}$$

which exponentially stabilizes the dynamics of the error $\boldsymbol{e} = \boldsymbol{q} - \boldsymbol{q}_d$ w.r.t. the desired trajectory $\boldsymbol{q}_d(t) \in \mathbb{R}^N$. The mappings $\boldsymbol{K}_{P,D} : \mathbb{R}^{N\times N} \to \mathbb{R}^{N\times N}$ should be designed to balance pure feedback with the model-based, mixed feedforward-feedback law $\boldsymbol{u}(\cdot)$ given the uncertainty quantifying covariance $\boldsymbol{\Sigma}_{\boldsymbol{\tau}} \succ \boldsymbol{0}$ arising from the learned data-driven model for (2).

Objective 2: At the same time, the nonlinear impedance $\boldsymbol{g}(\boldsymbol{q}) + \boldsymbol{D}(\dot{\boldsymbol{q}})\dot{\boldsymbol{q}}$ of the system (2) is to be preserved by (3) such that the closed-loop's impedance is comprised of $\boldsymbol{g}(\boldsymbol{e}) + \boldsymbol{D}(\dot{\boldsymbol{e}})\dot{\boldsymbol{e}}$ in addition to the uncertainty-adaptive injections.

For learning of the unknown system (1) and (2) based on a training dataset

$$\mathcal{D} = \{\boldsymbol{X}, \boldsymbol{Y}\} \tag{4}$$

we consider the following measurement scenario, introduced informally for the sake of space. The interested reader is referred to [21] for the accurate version. The unknown Lagrangian function $L(\boldsymbol{q}, \dot{\boldsymbol{q}})$ from (1) is approximated by a data-driven estimate $\hat{L}(\boldsymbol{q}, \dot{\boldsymbol{q}})$, which is physically consistent [1] and used in the model-based controller $\boldsymbol{u}(\cdot)$ in (3). For this, we assume access to noisefree position $\boldsymbol{q}_i$ and velocity observations $\dot{\boldsymbol{q}}_i$, $i = 1, \ldots, D$ with $D \in \mathbb{N}$, and to potentially noisy acceleration $\ddot{\boldsymbol{q}}_i + \boldsymbol{z}_i$, $\boldsymbol{z}_i \sim \mathcal{N}(\boldsymbol{0}, \boldsymbol{\Sigma}_{\boldsymbol{z}_i})$, and torque measurements

$$\boldsymbol{y}_i = \boldsymbol{\tau}_i(\boldsymbol{q}_i, \dot{\boldsymbol{q}}_i, \ddot{\boldsymbol{q}}_i) + \boldsymbol{\theta}_i\,, \quad \boldsymbol{\theta}_i \sim \mathcal{N}(\boldsymbol{0}, \boldsymbol{\Sigma}_{\boldsymbol{\theta}_i})\,. \tag{5}$$

The noise processes $\{\boldsymbol{z}_i\}$ and $\{\boldsymbol{\theta}_i\}$ are white, zero-mean, uncorrelated, and have known covariance matrices $\boldsymbol{\Sigma}_{\boldsymbol{z}_i}$ and $\boldsymbol{\Sigma}_{\boldsymbol{\theta}_i}$, respectively. After collecting all D observations at input positions $\boldsymbol{X} = [\boldsymbol{q}_i^\top, \dot{\boldsymbol{q}}_i{}^\top, \ddot{\boldsymbol{q}}_i^\top + \boldsymbol{z}_i{}^\top]$ with analogous output matrix $\boldsymbol{Y} = [\boldsymbol{y}_i^\top]$, we obtain the dataset (4) used for learning.

III. GP Regression for Lagrangian Systems

This section briefly overviews our employed modeling framework from [1] and [21]. For a complete introduction, particularly to GPs, the reader is referred to the literature [26], [27], [28], [29].

A. Background: GP Framework

A GP can be interpreted as a Gaussian distribution extended from random variables to functions. By construction, it thus inherits the properties of the Normal distribution, such that, e.g., conditioning and marginalization remain Gaussian. Considering vector-valued functions $\boldsymbol{f} : \mathbb{R}^M \to \mathbb{R}^N$, a GP with mean $\boldsymbol{m}(\boldsymbol{x})$ and covariance or kernel $\boldsymbol{K}(\boldsymbol{x}, \boldsymbol{x}')$ is denoted by

$$\boldsymbol{f}(\boldsymbol{x}) \sim \mathcal{GP}\left(\boldsymbol{m}(\boldsymbol{x}), \boldsymbol{K}(\boldsymbol{x}, \boldsymbol{x}')\right)\,.$$

Given D observations $\boldsymbol{y}_i = \boldsymbol{f}(\boldsymbol{x}_i) + \boldsymbol{\epsilon}_i$, $i = 1, \ldots, D$, perturbed by white noise $\boldsymbol{\epsilon}_i \sim \mathcal{N}(\boldsymbol{0}, \boldsymbol{\Sigma}_{\boldsymbol{\epsilon}_i})$, GPs assume a prior distribution of the function $\boldsymbol{f}$, specified by $\boldsymbol{m}$ and $\boldsymbol{K}$, and then leverage the resulting predictive distribution by using Bayes' rule. Equivalently, from the function-space view, GPs exploit the joint Gaussian distribution of the measurements $\boldsymbol{Y}$ and a desired estimate $\boldsymbol{f}(\boldsymbol{x})$ by conditioning on the former, giving rise to the posterior mean $\boldsymbol{\mu}_{\boldsymbol{f}}(\boldsymbol{x}) \equiv \mathrm{E}[\boldsymbol{f}(\boldsymbol{x})|\boldsymbol{Y}, \boldsymbol{X}]$ and covariance $\boldsymbol{\Sigma}_{\boldsymbol{f}}(\boldsymbol{x}) \equiv \mathrm{Var}[\boldsymbol{f}(\boldsymbol{x})|\boldsymbol{Y}, \boldsymbol{X}]$ given in turn by

$$\boldsymbol{\mu}_{\boldsymbol{f}}(\boldsymbol{x}) = \boldsymbol{m}(\boldsymbol{x}) + \boldsymbol{k}^\top(\boldsymbol{x})\left(\boldsymbol{K}(\boldsymbol{X}) + \boldsymbol{\Sigma}_{\boldsymbol{\epsilon}}\right)^{-1} \mathrm{vec}(\boldsymbol{Y} - \boldsymbol{m}(\boldsymbol{X})) \tag{6a}$$

$$\boldsymbol{\Sigma}_{\boldsymbol{f}}(\boldsymbol{x}) = \boldsymbol{K}(\boldsymbol{x}, \boldsymbol{x}) - \boldsymbol{k}^\top(\boldsymbol{x})\left(\boldsymbol{K}(\boldsymbol{X}) + \boldsymbol{\Sigma}_{\boldsymbol{\epsilon}}\right)^{-1} \boldsymbol{k}(\boldsymbol{x}) \tag{6b}$$

with $\boldsymbol{k}(\boldsymbol{x}) = \boldsymbol{K}(\boldsymbol{X}, \boldsymbol{x})$ and where $\boldsymbol{K}(\boldsymbol{X})$ and $\boldsymbol{\Sigma}_{\boldsymbol{\epsilon}}$ are the multidimensional Gramian and noise covariance block matrices, respectively.

Authorized licensed use limited to: TU Delft Library. Downloaded on July 10,2026 at 10:21:06 UTC from IEEE Xplore. Restrictions apply.

The kernel matrix $\boldsymbol{K}(\boldsymbol{x},\boldsymbol{x}') \in \mathbb{R}^{N\times N}$ is positive semidefinite [29] for any $\boldsymbol{x},\boldsymbol{x}'$, quantifies the correlation or similarity between the components of $\boldsymbol{f}(\boldsymbol{x})$ and $\boldsymbol{f}(\boldsymbol{x}')$, and determines higher level functional properties, such as smoothness. Dependent on so-called hyperparameters, the marginal likelihood [26] is mostly maximized numerically to maximize the probability of observing the measured outputs at the given inputs.

Also, GPs have the key property that linear transformations remain GPs [27] due to their construction based on the expectation. Thus, applying a linear transformation operator $\mathcal{T}_{\boldsymbol{x}}$, e.g., differentiation or integration, yields a GP again [30]

$$\mathcal{T}_{\boldsymbol{x}}\boldsymbol{f}(\boldsymbol{x}) \sim \mathcal{GP}\left(\mathcal{T}_{\boldsymbol{x}}\boldsymbol{m}(\boldsymbol{x}), \mathcal{T}_{\boldsymbol{x}}\boldsymbol{K}(\boldsymbol{x},\boldsymbol{x}')\mathcal{T}_{\boldsymbol{x}'}^{\top}\right). \tag{7}$$

Having introduced the basic framework of GPs, we now describe their unification with Lagrangian first-order principles.

B. Background: L-GP

1) Modeling Approach: The core concept we apply is to physically constrain the employed GP distribution's function space. For this, we exploit the Lagrangian-differential operator

$$\mathcal{L}_{\boldsymbol{q}} := \left(\frac{\partial}{\partial \dot{\boldsymbol{q}}^{\top}}\ddot{\boldsymbol{q}} + \frac{\partial}{\partial \boldsymbol{q}^{\top}}\dot{\boldsymbol{q}}\right)\frac{\partial}{\partial \dot{\boldsymbol{q}}} - \frac{\partial}{\partial \boldsymbol{q}} \tag{8}$$

to induce the multidimensional dynamics (2) from a scalar GP for the uncertain Lagrangian function $L(\boldsymbol{q},\dot{\boldsymbol{q}})$ with mean m_L and kernel k_L. Thus, Hamilton's principle of Least Action is deterministically guaranteed by embedding the differential equation structure (1) into the GP. Since the transformation (8) is linear [27], we can leverage (7) and denote

$$\boldsymbol{\tau}_c(\boldsymbol{q},\dot{\boldsymbol{q}},\ddot{\boldsymbol{q}}) \sim \mathcal{GP}\left(\mathcal{L}_{\boldsymbol{q}}m_L(\boldsymbol{q},\dot{\boldsymbol{q}}), \mathcal{L}_{\boldsymbol{q}}\mathcal{L}_{\boldsymbol{q}'}^{\top}k_L(\boldsymbol{q},\dot{\boldsymbol{q}},\boldsymbol{q}',\dot{\boldsymbol{q}}')\right) \tag{9}$$

resembling a multidimensional GP for $\boldsymbol{\tau}_c$ in (1). Incorporating generalized friction in compliance with Lagrangian mechanics into structured model learning is nontrivial [6]. However, the specific matrix-vector structure asserted in Assumption 4 can be enforced with the covariance [1]

$$\boldsymbol{K}_f(\dot{\boldsymbol{q}},\dot{\boldsymbol{q}}') = \operatorname{diag}(\dot{\boldsymbol{q}})\boldsymbol{K}_d(\dot{\boldsymbol{q}},\dot{\boldsymbol{q}}')\operatorname{diag}(\dot{\boldsymbol{q}}') \tag{10}$$

for which positive-semidefiniteness and passivity guarantees can be provided [31]. Therefore, combining the dissipative GP $\boldsymbol{\tau}_f \sim \mathcal{GP}(\boldsymbol{m}_f,\boldsymbol{K}_f)$ for prior mean $\boldsymbol{m}_f$ and kernel (10) with the conservative torques (9), we arrive at the multidimensional composite GP model

$$\boldsymbol{\tau} = \boldsymbol{\tau}_c + \boldsymbol{\tau}_f \sim \mathcal{GP}\left(\underbrace{\mathcal{L}_{\boldsymbol{q}}m_L + \boldsymbol{m}_f}_{=\boldsymbol{m}_{\boldsymbol{\tau}}}, \underbrace{\mathcal{L}_{\boldsymbol{q}}\mathcal{L}_{\boldsymbol{q}'}^{\top}k_L + \boldsymbol{K}_f}_{=\boldsymbol{K}_{\boldsymbol{\tau}}}\right). \tag{11}$$

2) Energy Structuring: The L-GP in (8) and (9) is split up further into its energy components, cf., Assumption 1, each considered as independent GPs again, i.e., $T,G,U \sim \mathcal{GP}$ with $V = G + U$, where G and U denote the underlying gravitational and elastic energies, respectively. For the kinetic energy, we make use of a specific kernel structure [21]

$$k_T = \frac{1}{4}\dot{\boldsymbol{q}}^{\top}\operatorname{diag}(\dot{\boldsymbol{q}}')\boldsymbol{\Theta}_M(\boldsymbol{q},\boldsymbol{q}')\operatorname{diag}(\dot{\boldsymbol{q}}')\dot{\boldsymbol{q}} \tag{12}$$

with the Cholesky decomposed covariance $\boldsymbol{\Theta}_M = \boldsymbol{R}_M^{\top}\boldsymbol{R}_M$ and upper right triangular $\boldsymbol{R}_M(\boldsymbol{q},\boldsymbol{q}')$. $U(\boldsymbol{q})$ is constrained analogously. Contrary to deterministically enforcing positive definiteness as in [32] via Cholesky decomposition of the output matrix, e.g., the mass-inertia, this approach only deterministically preserves the energies' quadratic form in order to stochastically preserve Gaussianity. In this manner, the mass-inertia matrix remains a (symmetric) matrix-valued GP.

Due to the structurally enforced constraints (8)–(12), the posterior $\hat{\boldsymbol{\tau}} := \boldsymbol{\mu}_{\boldsymbol{\tau}} = \mathrm{E}[\boldsymbol{\tau}|\boldsymbol{Y},\boldsymbol{X}]$ from (6a) of the L-GP (11) becomes [21]

$$\hat{\boldsymbol{\tau}}(\boldsymbol{q},\dot{\boldsymbol{q}},\ddot{\boldsymbol{q}}) = \hat{\boldsymbol{M}}(\boldsymbol{q})\ddot{\boldsymbol{q}} + \hat{\boldsymbol{C}}(\boldsymbol{q},\dot{\boldsymbol{q}})\dot{\boldsymbol{q}} + \hat{\boldsymbol{g}}(\boldsymbol{q}) + \hat{\boldsymbol{D}}(\dot{\boldsymbol{q}})\dot{\boldsymbol{q}}. \tag{13}$$

The (symmetric) posterior mass-inertia estimate $\hat{\boldsymbol{M}} : \mathbb{R}^N \to \mathbb{R}^{N\times N}$ is guaranteed to be positive definite with high probability [21]. Also, $\hat{\boldsymbol{C}}$ is here the Coriolis estimate constructed as $\hat{\boldsymbol{C}}(\boldsymbol{q},\dot{\boldsymbol{q}}) := \frac{1}{2}\left(\frac{\partial^2\hat{T}}{\partial\dot{\boldsymbol{q}}\partial\boldsymbol{q}^{\top}} + \dot{\hat{\boldsymbol{M}}}(\boldsymbol{q}) - \frac{\partial^2\hat{T}}{\partial\boldsymbol{q}\partial\dot{\boldsymbol{q}}^{\top}}\right)$ [33]. These first two terms, combined with the potential force estimate $\hat{\boldsymbol{g}}(\boldsymbol{q}) = \frac{\partial}{\partial\boldsymbol{q}}(\hat{G}+\hat{U})$, also comprise the posterior $\hat{\boldsymbol{\tau}}_c := \boldsymbol{\mu}_{\boldsymbol{\tau}_c}$ of the conservative torque GP (9), and are provably lossless [21], deterministically. Note that the dissipative L-GP's covariance estimate $\boldsymbol{\Sigma}_{\boldsymbol{\tau}} \equiv \operatorname{Var}[\boldsymbol{\tau}|\boldsymbol{Y},\boldsymbol{X}]$ from (11) also follows from (6b) with the kernel matrix $\boldsymbol{K}_{\boldsymbol{\tau}} = \mathcal{L}_{\boldsymbol{q}}\mathcal{L}_{\boldsymbol{q}'}^{\top}k_L + \boldsymbol{K}_f$. Having laid out the modeling framework, we can now proceed with the first contributions of this article.

IV. Control Design

In the following, we present our proposed feedback control architecture targeting accurate yet efficient trajectory tracking.

A. Natural Structure-Preserving Control

As illustrated in Fig. 1, we propose a structure-preserving control scheme based on projections according to

$$\begin{aligned}\boldsymbol{\tau} = {}& \hat{\boldsymbol{M}}(\boldsymbol{q})\ddot{\boldsymbol{q}}_d + \hat{\boldsymbol{C}}(\boldsymbol{q},\dot{\boldsymbol{q}})\dot{\boldsymbol{q}}_d + \left(\boldsymbol{I} - h(\boldsymbol{e}^{\top}\hat{\boldsymbol{g}}_{\boldsymbol{q}})\boldsymbol{P}_{\boldsymbol{e}}\right)\hat{\boldsymbol{g}}_{\boldsymbol{q}} - \boldsymbol{g}_d(\boldsymbol{e},t) \\ & + \left(\boldsymbol{I} - h(\dot{\boldsymbol{e}}^{\top}\hat{\boldsymbol{d}}_{\dot{\boldsymbol{q}}})\boldsymbol{P}_{\dot{\boldsymbol{e}}}\right)\hat{\boldsymbol{d}}_{\dot{\boldsymbol{q}}} - \boldsymbol{d}_d(\dot{\boldsymbol{e}},t)\end{aligned} \tag{14}$$

where $\boldsymbol{e} = \boldsymbol{q} - \boldsymbol{q}_d$ is the position error based on the desired reference trajectory $\boldsymbol{q}_d(t)$, and $\hat{\boldsymbol{M}}(\boldsymbol{q}), \hat{\boldsymbol{C}}(\boldsymbol{q},\dot{\boldsymbol{q}}), \hat{\boldsymbol{g}}(\boldsymbol{q}) =: \hat{\boldsymbol{g}}_{\boldsymbol{q}}$, and $\hat{\boldsymbol{D}}(\dot{\boldsymbol{q}})\dot{\boldsymbol{q}} =: \hat{\boldsymbol{d}}_{\dot{\boldsymbol{q}}}$ are the learned inertia, Coriolis matrix, gravity and friction, respectively, as defined in (13). The Heaviside step function $h(x)$ is given by

$$h(x) = \frac{1}{2}\left(1 + \operatorname{sign}(x)\right) \tag{15}$$

for $x \in \mathbb{R}$, and $\boldsymbol{P}_{\boldsymbol{e}} \in \mathbb{R}^{N\times N}$ is the orthogonal projector [34] onto the 1-D space spanned by $\boldsymbol{e} \in \mathbb{R}^N$

$$\boldsymbol{P}_{\boldsymbol{e}} = \frac{\boldsymbol{e}\boldsymbol{e}^{\top}}{\|\boldsymbol{e}\|^2}. \tag{16}$$

The methodology behind (14) is to alternate the well-known standard PD+ controller [22] to compensate potential and dissipative forces stemming from, e.g., gravity and friction, respectively, only when necessary. Assume, for instance, $\boldsymbol{e}^{\top}\hat{\boldsymbol{g}}_{\boldsymbol{q}} > 0$ and $\dot{\boldsymbol{e}}^{\top}\hat{\boldsymbol{d}}_{\dot{\boldsymbol{q}}} > 0$, meaning that both vector quantities point in

Authorized licensed use limited to: TU Delft Library. Downloaded on July 10,2026 at 10:21:06 UTC from IEEE Xplore. Restrictions apply.

the direction of the error quantities $\boldsymbol{e}$ and $\dot{\boldsymbol{e}}$. Then, (14) can be simplified with $\boldsymbol{e}^\top \hat{\boldsymbol{g}}_{\boldsymbol{q}} > 0\,,\ \dot{\boldsymbol{e}}^\top \hat{\boldsymbol{d}}_{\dot{\boldsymbol{q}}} > 0$ to

$$\boldsymbol{\tau} = \hat{\boldsymbol{M}}(\boldsymbol{q})\ddot{\boldsymbol{q}}_d + \hat{\boldsymbol{C}}(\boldsymbol{q},\dot{\boldsymbol{q}})\dot{\boldsymbol{q}}_d + \hat{\boldsymbol{g}}_{\perp \boldsymbol{e}}(\boldsymbol{q}) + \hat{\boldsymbol{d}}_{\perp \dot{\boldsymbol{e}}}(\dot{\boldsymbol{q}}) - \boldsymbol{g}_d - \boldsymbol{d}_d$$

with $\hat{\boldsymbol{g}}_{\perp \boldsymbol{e}} = \boldsymbol{P}_{\boldsymbol{e}}^{\perp}\hat{\boldsymbol{g}}$ and $\hat{\boldsymbol{d}}_{\perp \dot{\boldsymbol{e}}} = \boldsymbol{P}_{\dot{\boldsymbol{e}}}{}^{\perp}\hat{\boldsymbol{d}}$, where $\boldsymbol{P}_{\boldsymbol{e}}^{\perp} = \boldsymbol{I} - \boldsymbol{P}_{\boldsymbol{e}}$. Thus, if either of the model-based estimates points in the direction of the respective error, then the parallel components are preserved and exploited, while the orthogonal subvectors are canceled, cf., Fig. 1. In this way, we can improve the actuation efficiency of [22]. Note that this is also implicitly achieved in part by combining the PD+ controller [22] with the increased modeling accuracy of the L-GP framework [21]. Although, in total, four pairings of the impedance $\boldsymbol{g}(\boldsymbol{q}) + \boldsymbol{D}(\boldsymbol{q},\dot{\boldsymbol{q}})\dot{\boldsymbol{q}}$ with positional and velocity errors would be possible, our usage of the two in (14) leads to variable yet natural PD gains exclusively depending on the error variable they multiply, a typical design approach for adaptive feedback gains [35]. Also, note that the controller (14) is continuous w.r.t. the arguments of the Heaviside functions since these are zero only when the respective vectors become orthogonal. Due to the multiplication with the respective projections, the parallel subvectors also become zero in these instances, enforcing a continuous mapping. Enforcing differentiability would also be possible via, e.g., a redefinition of the backward pass of the Heaviside function (15), as in [36].

In the following section, we elaborate on the role of the remaining quantities in the controller (14), i.e., the desired potential and dissipation forces $\boldsymbol{g}_d(\boldsymbol{e},t)$ and $\boldsymbol{d}_d(\dot{\boldsymbol{e}},t)$, respectively.

B. Uncertainty-Based Potential Shaping and Damping Injection: Feedforward-Feedback Balancing

In order to obtain a structurally preserved closed-loop, we propose a reference potential and dissipation given by

$$\boldsymbol{g}_d(\boldsymbol{e},t) = \hat{\boldsymbol{g}}(\boldsymbol{e}) + \boldsymbol{K}_P(\boldsymbol{\Sigma}_{\boldsymbol{\tau}}(t))\boldsymbol{e} \tag{17a}$$

$$\boldsymbol{d}_d(\dot{\boldsymbol{e}},t) = \hat{\boldsymbol{d}}(\dot{\boldsymbol{e}}) + \boldsymbol{K}_D(\boldsymbol{\Sigma}_{\boldsymbol{\tau}}(t))\dot{\boldsymbol{e}} \tag{17b}$$

with learned gravity $\hat{\boldsymbol{g}}(\cdot)$ and friction $\hat{\boldsymbol{d}}(\cdot)$ estimates from (13) evaluated at position and velocity errors, respectively, and (time-variant) uncertainty-adaptive energy shaping and damping injection based on the covariance matrix $\boldsymbol{\Sigma}_{\boldsymbol{\tau}}$ and positive definite matrix functions $\boldsymbol{K}_{P,D} : \mathbb{R}^{N\times N} \to \mathbb{R}^{N\times N}$. Aside from achieving a measure of robustness by this design approach due to the smaller dynamical intervention, this is also particularly beneficial upon potential interactions with the environment, such as for a soft robot remaining inherently compliant due to its preserved softness [17], instead of being stiffened by feedback. To still be able to accurately achieve the control task, the uncertainty-adaptive gains $\boldsymbol{K}_{P,D}(\boldsymbol{\Sigma}_{\boldsymbol{\tau}})$ have the purpose of implementing an automatic balancing between feedforward and feedback elements.

Thus, for uncertainty-adaptive balancing between the feedback and feedforward elements in (14)–(17), we propose a specific structure for the matrix gains $\boldsymbol{K}_{P,D}$ given by

$$\boldsymbol{K}(\boldsymbol{\Sigma}_{\boldsymbol{\tau}}) := \boldsymbol{K}_1\left(\boldsymbol{I} - \left[\boldsymbol{K}_3(\boldsymbol{K}_2 + \boldsymbol{\Sigma}_{\boldsymbol{\tau}})\boldsymbol{K}_3 + \boldsymbol{K}_1\right]^{-1}\boldsymbol{K}_1\right) \tag{18}$$

with constant, positive definite matrices $\boldsymbol{K}_{1-3} \succ \boldsymbol{0}$. Using variational principles for the eigenvalues of symmetric operators [37], we can provide a guarantee on the user-definably bounded interval in which the eigenvalues of $\boldsymbol{K}(\boldsymbol{\Sigma}_{\boldsymbol{\tau}})$ lie.

Lemma 1: The uncertainty-adaptive gain (18) with constant $\boldsymbol{0} \prec \underline{k}_i\boldsymbol{I} \prec \boldsymbol{K}_i \prec \bar{k}_i\boldsymbol{I}$, where $\underline{k}_i, \bar{k}_i \in \mathbb{R}^+$ for $i = 1,2,3$, is guaranteed to fulfill the linear matrix inequalities

$$\frac{1}{(\underline{k}_3^2\underline{k}_2)^{-1} + \underline{k}_1^{-1}}\boldsymbol{I} \prec \boldsymbol{K}(\boldsymbol{\Sigma}_{\boldsymbol{\tau}}) \prec \bar{k}_1\boldsymbol{I}. \tag{19}$$

Proof: For the proof of the bounds for $\boldsymbol{K}(\boldsymbol{\Sigma}_{\boldsymbol{\tau}})$, we reformulate (18) to $\boldsymbol{K}(\boldsymbol{\Sigma}_{\boldsymbol{\tau}}) = (\boldsymbol{K}_1^{-1} + \boldsymbol{K}_3^{-1}(\boldsymbol{K}_2 + \boldsymbol{\Sigma}_{\boldsymbol{\tau}})^{-1}\boldsymbol{K}_3^{-1})^{-1}$ by making use of the matrix inversion lemma [38, ch. 4.3]. The inequalities (19) then directly follow from [1, Lemma 3] after utilizing $\boldsymbol{\lambda}(\boldsymbol{A}^{-1}) = \boldsymbol{\lambda}^{-1}(\boldsymbol{A})$, $\boldsymbol{A} \in \mathbb{R}^{N\times N}$. ■

Using (19), one can enforce the spectrum $\boldsymbol{\lambda}(\boldsymbol{K}(\boldsymbol{\Sigma}_{\boldsymbol{\tau}}))$ of the adaptive gain (18) to lie in an interval on the axis of positive reals, where $\bar{k}_1$ defines the maximum gain for $\bar{\lambda}(\boldsymbol{\Sigma}_{\boldsymbol{\tau}}) \to \infty$. We gather that $\boldsymbol{K}_3$ defines the scaling manner in which the gain follows $\boldsymbol{\Sigma}_{\boldsymbol{\tau}}$. Moreover, $\boldsymbol{K}_2$ is typically chosen such that $0 < \underline{k}_2 << 1$ to specify a small positive minimum gain while also improving the condition number of the covariance. A desired positive lower bound $0 < \underline{k} < \bar{k} = \underline{k}_1$ can be achieved by, e.g., fixing $\underline{k}_1$ and $\underline{k}_2$ and setting $1/\underline{k}_3 = \sqrt{\underline{k}_2(1/\underline{k} - 1/\underline{k}_1)}$. Having motivated and legitimated the design principles behind our proposed control law (14)–(17), we now proceed to analyze the stability and convergence of the resulting closed-loop error dynamics in the following section.

C. Overall Algorithm

The pseudocode of the overall algorithm involving the full combination of all proposed methods is given in Algorithm 1.

D. Exponential Stability Analysis

Due to the data-driven nature of the model, we consider its uncertainty probabilistically to arrive at a stability guarantee holding with high probability $1-\delta$, where $0 < \delta \ll 1$. As a prerequisite, we require the following assumption.

Assumption 5: The unknown torques $\boldsymbol{\tau}(\boldsymbol{q},\dot{\boldsymbol{q}},\ddot{\boldsymbol{q}})$ are a sample drawn from the L-GP (11) of which $D \in \mathbb{N}$ noisy observations have been collected according to (5).

The force error $\tilde{\boldsymbol{\tau}} = \boldsymbol{\tau} - \hat{\boldsymbol{\tau}}$ can now be bounded probabilistically based on [1, Lemma 2], permitting a deterministic analysis of the closed-loop error dynamics

$$\hat{\boldsymbol{M}}(\boldsymbol{q})\ddot{\boldsymbol{e}} + \hat{\boldsymbol{C}}(\boldsymbol{q},\dot{\boldsymbol{q}})\dot{\boldsymbol{e}} + h(\dot{\boldsymbol{e}}^\top\hat{\boldsymbol{d}}(\dot{\boldsymbol{q}}))\frac{\dot{\boldsymbol{e}}^\top\hat{\boldsymbol{d}}(\dot{\boldsymbol{q}})}{\|\dot{\boldsymbol{e}}\|^2}\dot{\boldsymbol{e}} + \boldsymbol{d}_d(\dot{\boldsymbol{e}},t)$$
$$+ h(\boldsymbol{e}^\top\hat{\boldsymbol{g}}(\boldsymbol{q}))\frac{\boldsymbol{e}^\top\hat{\boldsymbol{g}}(\boldsymbol{q})}{\|\boldsymbol{e}\|^2}\boldsymbol{e} + \boldsymbol{g}_d(\boldsymbol{e},t) + \tilde{\boldsymbol{\tau}} = \boldsymbol{0} \tag{20}$$

resulting from the controller (14) applied to the system (2).

Authorized licensed use limited to: TU Delft Library. Downloaded on July 10,2026 at 10:21:06 UTC from IEEE Xplore. Restrictions apply.

Algorithm 1: Natural $\boldsymbol{\Sigma}$-Adaptive L-GP var-nat-PD+.

OFFLINE:
Inputs: training data measurements $\mathcal{D}$
Compute: hyperparameters $\boldsymbol{\psi}$ locally minimizing marginal likelihood or least-squares approximation
ONLINE:
Inputs: initial system state $\boldsymbol{q}(0), \dot{\boldsymbol{q}}(0)$
At each time t**:**
Compute: L-GP mean estimates $\hat{\boldsymbol{M}}, \hat{\boldsymbol{C}}, \hat{\boldsymbol{g}}, \hat{\boldsymbol{d}}$ at $\boldsymbol{q}(t), \dot{\boldsymbol{q}}(t)$
Evaluate: tracking error $\boldsymbol{e}(t) = \boldsymbol{q}(t) - \boldsymbol{q}_d(t)$ and $\dot{\boldsymbol{e}}(t)$
if projection $\boldsymbol{e}^\top \hat{\boldsymbol{g}} > 0$ **then**
    only compensate orthogonal $\hat{\boldsymbol{g}}_{\perp \boldsymbol{e}}$ in control law $\boldsymbol{\tau}$
else
    use full $\hat{\boldsymbol{g}}$ in control law $\boldsymbol{\tau}$
end if
if projection $\dot{\boldsymbol{e}}^\top \hat{\boldsymbol{d}} > 0$ **then**
    only compensate orthogonal $\hat{\boldsymbol{d}}_{\perp \dot{\boldsymbol{e}}}$ in control law $\boldsymbol{\tau}$
else
    use full $\hat{\boldsymbol{d}}$ in control law $\boldsymbol{\tau}$
end if
Compute: L-GP covariance $\boldsymbol{\Sigma}_{\boldsymbol{\tau}}(t)$ and adapt $\boldsymbol{K}_P, \boldsymbol{K}_D$
Apply control $\boldsymbol{\tau} = \boldsymbol{u} - \boldsymbol{K}_P \boldsymbol{e} - \boldsymbol{K}_D \dot{\boldsymbol{e}}$

Theorem 1 (Natural $\boldsymbol{\Sigma}$-adaptive PD+): The L-GP-based closed-loop (20) is exponentially stable for $\delta \in (0,1)$

$$\Pr\left\{ \|[\boldsymbol{e}, \dot{\boldsymbol{e}}](t)\| \leq \varrho(t) + c_0 e^{-\int_{t_0}^{t} \alpha(\tau) d\tau} \right\} = 1 - \delta \tag{21}$$

with convergence rate $\alpha(t) \geq \underline{\alpha} \in \mathbb{R}^+$ and radius $\varrho(t)$ given by

$$\alpha(t) = \frac{\lambda(\alpha(t), t)(\|\boldsymbol{e}\|^2 + \|\dot{\boldsymbol{e}}\|^2) + \varepsilon(\boldsymbol{e}^\top \hat{\boldsymbol{g}}_{\boldsymbol{e}} + \nu_{\boldsymbol{e}} + \omega_{\dot{\boldsymbol{e}}}) + \nu_{\dot{\boldsymbol{e}}} + \omega_{\boldsymbol{e}}}{\hat{G}(\boldsymbol{e})} \tag{22}$$

$$\varrho(t) = \Delta \sqrt{\frac{\varepsilon/\vartheta + 1/\varphi}{2\underline{\mu}(t)}}. \tag{23}$$

Here, $\hat{G}(\boldsymbol{e})$ is the L-GP's potential energy, $\lambda(\alpha(t), t)$ is an eigenvalue function, $\nu_{\boldsymbol{e}} = h(\boldsymbol{e}^\top \hat{\boldsymbol{g}}_{\boldsymbol{q}}) \boldsymbol{e}^\top \hat{\boldsymbol{g}}_{\boldsymbol{q}} \geq 0$, $\nu_{\dot{\boldsymbol{e}}} = h(\dot{\boldsymbol{e}}^\top \hat{\boldsymbol{d}}_{\dot{\boldsymbol{q}}}) \dot{\boldsymbol{e}}^\top \hat{\boldsymbol{d}}_{\dot{\boldsymbol{q}}} \geq 0$, and $\omega_{\boldsymbol{e}} = h(\boldsymbol{e}^\top \hat{\boldsymbol{g}}_{\boldsymbol{q}}) \dot{\boldsymbol{e}}^\top \boldsymbol{P}_{\boldsymbol{e}} \hat{\boldsymbol{g}}_{\boldsymbol{q}}$, $\omega_{\dot{\boldsymbol{e}}} = h(\dot{\boldsymbol{e}}^\top \hat{\boldsymbol{d}}_{\dot{\boldsymbol{q}}}) \boldsymbol{e}^\top \boldsymbol{P}_{\dot{\boldsymbol{e}}} \hat{\boldsymbol{d}}_{\dot{\boldsymbol{q}}}$. Aside from the constants $\varepsilon, \vartheta, \Delta \in \mathbb{R}^+$, the radius (23) is determined by

$$\underline{\mu}(t) = \frac{\kappa + \underline{\hat{m}}(t)}{2} - \sqrt{\left[\frac{\kappa - \underline{\hat{m}}(t)}{2}\right]^2 + [\varepsilon \underline{\hat{m}}(t)]^2} + \frac{2\hat{G}(\boldsymbol{e})}{\|\boldsymbol{e}\|^2 + \|\dot{\boldsymbol{e}}\|^2}. \tag{24}$$

The virtual stiffness $\kappa \in \mathbb{R}^+$ and scale $\varphi \in \mathbb{R}^+$ are given by

$$\kappa = \underline{k}_P + \varepsilon(\underline{d} - \underline{\alpha} \hat{m}_\Sigma) \tag{25a}$$

$$\varphi = 2\left[\underline{d} - \varepsilon\left(\underline{k}_P - \frac{\vartheta}{2}\right) + \underline{\alpha}\kappa\right] - (\varepsilon + \underline{\alpha})\hat{m}_\Sigma \tag{25b}$$

where $\underline{d} = \hat{\underline{d}} + \underline{k}_D$ and $\hat{m}_\Sigma = \underline{\hat{m}} + \bar{\hat{m}}$ are constant worst-case bounds, i.e., $\underline{d}\boldsymbol{I} \preceq \hat{\boldsymbol{D}} + \boldsymbol{K}_D$ and $\underline{\hat{m}}\boldsymbol{I} \preceq \hat{\boldsymbol{M}} \preceq \bar{\hat{m}}\boldsymbol{I}$. The inequalities

$$\varepsilon < \min\left[\frac{\underline{d}}{\underline{k}_P - \vartheta/2 + \hat{m}_\Sigma}, \frac{\underline{d} - \underline{\alpha}\hat{m}_\Sigma}{2\bar{\hat{m}}} \times \left(1 + \sqrt{1 + \frac{4\bar{\hat{m}}^2 \underline{k}_P}{(\underline{d} - \underline{\alpha}\hat{m}_\Sigma)^2}}\right)\right] \tag{26a}$$

$$\vartheta < 2(\underline{k}_P + \hat{m}_\Sigma) \tag{26b}$$

$$\underline{\alpha} < \min\left[\frac{\underline{d}}{\hat{m}_\Sigma}, \alpha_0 + \sqrt{\alpha_0^2 + \frac{\underline{d} - \varepsilon(\underline{k}_P - \vartheta/2 + \hat{m}_\Sigma)}{\varepsilon \hat{m}_\Sigma}}\right] \tag{26c}$$

are fulfilled by the parameters ε, ϑ, and $\underline{\alpha}$ for validity of the statement, where $\alpha_0 := \frac{\underline{k}_P + \varepsilon \underline{d} - \hat{m}_\Sigma/2}{2\varepsilon \hat{m}_\Sigma}$.

Remark 2: Note that the implicit (22) can be solved explicitly for the rate $\alpha(t)$. An analytical expression, also for the eigenvalue function $\lambda : \mathbb{R}^+ \times \mathbb{R} \to \mathbb{R}$, is derived and given in the proof of Theorem 1.

For the proof of Theorem 1, we apply ideas from contraction theory [39], revolving around the problem of finding a coordinate transformation, to construct an optimal Lyapunov function, which allows the provision of a maximal convergence rate and a minimal ball radius. This enables the derivation of a strong theoretical guarantee, which depends on a conservative usage of Young's inequality only once each where it is inevitable, i.e., where position and velocity are multiplied with the force error. The repeated application of these conservative inequalities, as in, e.g., [11], for bounds on Lyapunov functions and Coriolis terms, can potentially lead to infeasible guarantees. To circumvent these issues, we build majorly on matrix analysis arguments.

1) Intermediate Results: *Lemma 2:* The symmetric coordinate metric

$$\boldsymbol{\mathcal{M}} = \begin{bmatrix} \boldsymbol{\mathcal{K}} & \varepsilon \hat{\boldsymbol{M}} \\ \varepsilon \hat{\boldsymbol{M}} & \hat{\boldsymbol{M}} \end{bmatrix} \tag{27}$$

with a real constant $\varepsilon \in \mathbb{R}$, design stiffness $\boldsymbol{0} \prec \underline{\kappa}\boldsymbol{I} \preceq \boldsymbol{\mathcal{K}} \preceq \bar{\kappa}\boldsymbol{I}$, and L-GP inertia estimate $\boldsymbol{0} \prec \underline{\hat{m}}\boldsymbol{I} \preceq \hat{\boldsymbol{M}} \preceq \bar{\hat{m}}\boldsymbol{I}$, is uniformly positive definite, i.e., $\boldsymbol{\mathcal{M}} \succ \boldsymbol{0} \forall t$, iff $|\varepsilon| < \sqrt{\underline{\kappa}/\bar{\hat{m}}}$. Moreover, the metric (27) is guaranteed to fulfill the linear matrix inequalities (LMIs)

$$\boldsymbol{0} \prec \underline{\mu}\boldsymbol{I} \preceq \boldsymbol{\mathcal{M}} \preceq \bar{\mu}\boldsymbol{I} \tag{28a}$$

$$\bar{\mu} = \frac{1}{2}\left(\bar{\kappa} + \bar{\hat{m}} \pm \sqrt{(\bar{\kappa} - \bar{\hat{m}})^2 + (2\varepsilon\bar{\hat{m}})^2}\right) \tag{28b}$$

for nonzero values $0 < |\varepsilon| < \sqrt{\underline{\hat{m}}\underline{\kappa}}/\bar{\hat{m}}$.

Proof: The proof is given in Appendix A. ■

Next, we provide an exact and necessary condition in the simplified case of an Euclidian virtual stiffness.

Corollary 1: For Euclidian $\boldsymbol{\mathcal{K}} = \kappa\boldsymbol{I} \succ \boldsymbol{0}$ with $\kappa \in \mathbb{R}^+$ and $\hat{\boldsymbol{m}} := \boldsymbol{\lambda}(\hat{\boldsymbol{M}})$, all eigenvalues of the metric (27) are given by

$$\boldsymbol{\lambda}(\boldsymbol{\mathcal{M}}) = \frac{1}{2}\left(\kappa + \hat{\boldsymbol{m}} \pm \sqrt{(\kappa - \hat{\boldsymbol{m}})^2 + (2\varepsilon\hat{\boldsymbol{m}})^2}\right) \tag{29}$$

Authorized licensed use limited to: TU Delft Library. Downloaded on July 10,2026 at 10:21:06 UTC from IEEE Xplore. Restrictions apply.

which are positive for $|\varepsilon| < \sqrt{\kappa/\bar{m}}$.

Proof: Please see Appendix B. ■

2) Proof of the Main Result: We are now ready to prove the main result.

Proof of Theorem 1: To find an optimal Lyapunov function allowing the provision of a maximally tight guarantee, let us first consider the generalized candidate

$$V(\boldsymbol{e},\dot{\boldsymbol{e}},t) = \frac{1}{2}\begin{bmatrix}\boldsymbol{e}^\top & \dot{\boldsymbol{e}}^\top\end{bmatrix}\boldsymbol{\mathcal{M}}(\boldsymbol{e},\dot{\boldsymbol{e}},t)\begin{bmatrix}\boldsymbol{e}\\ \dot{\boldsymbol{e}}\end{bmatrix} =: \frac{1}{2}\boldsymbol{z}^\top\boldsymbol{z} \tag{30}$$

representing the squared length of some adequately transformed error coordinates $\boldsymbol{z} := \boldsymbol{\Theta}\boldsymbol{x}$. Thus, we implicitly define a positive definite and continuously differentiable metric

$$\boldsymbol{\mathcal{M}}(\boldsymbol{e},\dot{\boldsymbol{e}},t) = \boldsymbol{\Theta}^\top\boldsymbol{\Theta} \tag{31}$$

in whose Riemann space the squared length of $\boldsymbol{x}^\top{:=}[\boldsymbol{e}^\top\ \dot{\boldsymbol{e}}^\top]$ is investigated. Next, we exploit the structure of (20) by reformulating to $\dot{\boldsymbol{x}} = \boldsymbol{A}(\boldsymbol{x},t)\boldsymbol{x} + \boldsymbol{\pi}(\boldsymbol{x},t)$ with

$$\boldsymbol{A}^\top(\boldsymbol{x},t) = \begin{bmatrix}\boldsymbol{0} & -\hat{\boldsymbol{M}}^{-1}\left(\frac{\nu_{\boldsymbol{e}}}{\|\boldsymbol{e}\|^2}\boldsymbol{I} + \hat{\boldsymbol{K}}_G + \boldsymbol{K}_P\right)\\ \boldsymbol{I} & -\hat{\boldsymbol{M}}^{-1}\left(\hat{\boldsymbol{C}} + \frac{\nu_{\dot{\boldsymbol{e}}}}{\|\dot{\boldsymbol{e}}\|^2}\boldsymbol{I} + \hat{\boldsymbol{D}} + \boldsymbol{K}_D\right)\end{bmatrix} \tag{32}$$

and perturbation term

$$\boldsymbol{\pi} = \begin{bmatrix}\boldsymbol{0}\\ -\hat{\boldsymbol{M}}^{-1}\tilde{\boldsymbol{\tau}}\end{bmatrix}.$$

For notational brevity, we have substituted $\nu_{\boldsymbol{e}}$ and $\nu_{\dot{\boldsymbol{e}}}$ from (22) here. Now, we directly use $\boldsymbol{A}$ and the full state $\boldsymbol{x}$ to find a metric (31) for which

$$\boldsymbol{\mathcal{F}} := \boldsymbol{A}^\top\boldsymbol{\mathcal{M}} + \boldsymbol{\mathcal{M}}\boldsymbol{A} + \dot{\boldsymbol{\mathcal{M}}} \preceq -2\alpha\boldsymbol{\mathcal{M}} \tag{33}$$

holds uniformly $\forall t$. Inspecting (32), we observe the benefit of multiplying with $\hat{\boldsymbol{M}}$ in the second line for reducing the complexity of satisfying (33). Therefore, (27) is postulated as a fitting metric, where we have introduced a stiffness $\boldsymbol{\mathcal{K}}$, which will be fully specified later on. In order to prove the result, we combine (33) from [39, Thm. 2] with [40, Thm. 2.1]. Thus, computing the derivative of (30) w.r.t. to (27) gives

$$\dot{V} = \frac{1}{2}\boldsymbol{x}^\top\boldsymbol{\mathcal{F}}\boldsymbol{x} + \boldsymbol{x}^\top\boldsymbol{\mathcal{M}}\boldsymbol{\pi} = \frac{1}{2}\boldsymbol{x}^\top\boldsymbol{\mathcal{F}}\boldsymbol{x} - (\varepsilon\boldsymbol{e}+\dot{\boldsymbol{e}})^\top\tilde{\boldsymbol{\tau}}.$$

Since $\tilde{\boldsymbol{\tau}}$ is a time-varying disturbance independent of the error states $\boldsymbol{x}$, we need to upper bound the second term to bring the entire expression into the form $\dot{V} \leq -2\alpha(V - \underline{V})$ with constant $\underline{V} > 0$ such that [40, Thm. 2.1] is applicable. Using the Cauchy–Schwarz, triangle and Young's inequalities

$$\begin{aligned}-(\varepsilon\boldsymbol{e}+\dot{\boldsymbol{e}})^\top\tilde{\boldsymbol{\tau}} &\leq (|\varepsilon|\|\boldsymbol{e}\| + \|\dot{\boldsymbol{e}}\|)\|\tilde{\boldsymbol{\tau}}\|\\ &\leq \frac{|\varepsilon|\vartheta}{2}\|\boldsymbol{e}\|^2 + \frac{\varphi}{2}\|\dot{\boldsymbol{e}}\|^2 + \left(\frac{|\varepsilon|}{\vartheta}+\frac{1}{\varphi}\right)\frac{\|\tilde{\boldsymbol{\tau}}\|^2}{2}\end{aligned} \tag{34}$$

follows for positive constants $\vartheta, \varphi \in \mathbb{R}^+$. Next, we include the first two summands into the quadratic expression w.r.t. $\boldsymbol{\mathcal{F}}$ and apply [1, Lemma 2] for $\beta\sqrt{\underline{\lambda}(\boldsymbol{\Sigma}_{\boldsymbol{\tau}}(t))} + s + Ld \leq \Delta\sqrt{\alpha(t)}$ to eliminate the time-dependence of the remaining bias. Thus

$$\begin{aligned}&\Pr\left\{\dot{V} \leq \frac{1}{2}\boldsymbol{x}^\top(\boldsymbol{\mathcal{F}} + |\varepsilon|\vartheta\boldsymbol{I}\oplus\varphi\boldsymbol{I})\boldsymbol{x} + \frac{\alpha}{2}\left(\frac{|\varepsilon|}{\vartheta}+\frac{1}{\varphi}\right)\Delta^2\right\}\\ &= 1-\delta\end{aligned}$$

which is equivalent to requiring for [40, Thm. 2.1] that

$$\Pr\left\{\dot{V} \leq -2\alpha(t)\left[V - \left(\frac{|\varepsilon|}{\vartheta}+\frac{1}{\varphi}\right)\frac{\Delta^2}{4}\right]\right\} = 1-\delta \tag{35}$$

given that the matrix inequality

$$\boldsymbol{A}^\top\boldsymbol{\mathcal{M}} + \boldsymbol{\mathcal{M}}\boldsymbol{A} + \dot{\boldsymbol{\mathcal{M}}} + |\varepsilon|\vartheta\boldsymbol{I}\oplus\varphi\boldsymbol{I} \preceq -2\alpha(t)\boldsymbol{\mathcal{M}} \tag{36}$$

is fulfilled deterministically. Here, note that we make use of an extension of [40, Thm. 2.1] based on Grönwall's inequality to include a more precise time-variant convergence rate $\alpha(t) \geq \underline{\alpha} \in \mathbb{R}^+$. Therefore, analyzing under which conditions (28a) and (36) hold is all that is left to prove exponential stability and convergence to the ball (21)–(23). The former, i.e., lower bound in (28a), is necessary for computing the ball's radius as

$$\varrho^2(t) = \frac{2\underline{V}}{\underline{\mu}(t)} = \frac{|\varepsilon|/\vartheta + 1/\varphi}{2\underline{\mu}(t)}\Delta^2 \tag{37}$$

for which Lemma 2 or Corollary 1 can be used, depending on the form of $\boldsymbol{\mathcal{K}}$. Proceeding with the latter condition, we plug (27) and (32) into (36), reformulate, and obtain

$$\boldsymbol{0} \preceq \begin{bmatrix}\underbrace{\varepsilon\boldsymbol{P}' - \alpha\boldsymbol{\mathcal{K}} - \frac{\dot{\boldsymbol{\mathcal{K}}}}{2} - \frac{|\varepsilon|\vartheta}{2}\boldsymbol{I}}_{=\boldsymbol{P}} & \underbrace{\frac{1}{2}\boldsymbol{B}' - \frac{\varepsilon}{2}\hat{\boldsymbol{C}}^\top}_{=\boldsymbol{B}}\\ \underbrace{\frac{1}{2}\boldsymbol{B}' - \frac{\varepsilon}{2}\hat{\boldsymbol{C}}}_{=\boldsymbol{B}^\top} & \underbrace{\boldsymbol{E}' - (\varepsilon+\alpha)\hat{\boldsymbol{M}} - \frac{\varphi}{2}\boldsymbol{I}}_{=\boldsymbol{E}}\end{bmatrix}$$

$$\boldsymbol{P}' = \frac{\nu_{\boldsymbol{e}}}{\|\boldsymbol{e}\|^2}\boldsymbol{I} + \hat{\boldsymbol{K}}_G + \boldsymbol{K}_P, \quad \boldsymbol{E}' = \frac{\nu_{\dot{\boldsymbol{e}}}}{\|\dot{\boldsymbol{e}}\|^2}\boldsymbol{I} + \hat{\boldsymbol{D}} + \boldsymbol{K}_D$$

$$\boldsymbol{B}' = \boldsymbol{P}' - \boldsymbol{\mathcal{K}} + \varepsilon(\boldsymbol{E}' - 2\alpha\hat{\boldsymbol{M}}). \tag{38}$$

Leveraging Schur complements [41] and symmetric eigenvalue principles [37], we can derive the sufficient conditions

$$\boldsymbol{P} \succ \boldsymbol{0} \Rightarrow \boldsymbol{E} \succeq \boldsymbol{B}^\top\boldsymbol{P}^{-1}\boldsymbol{B} \Leftrightarrow \underline{\lambda}(\boldsymbol{E}) \geq \frac{[\bar{\lambda}(\boldsymbol{B}') + |\varepsilon|\|\hat{\boldsymbol{C}}\|]^2}{4\underline{\lambda}(\boldsymbol{P})}$$

$$\boldsymbol{E} \succ \boldsymbol{0} \Rightarrow \boldsymbol{P} \succeq \boldsymbol{B}\boldsymbol{E}^{-1}\boldsymbol{B}^\top \Leftrightarrow \underline{\lambda}(\boldsymbol{P}) \geq \frac{[\bar{\lambda}(\boldsymbol{B}') + |\varepsilon|\|\hat{\boldsymbol{C}}\|]^2}{4\underline{\lambda}(\boldsymbol{E})}$$

which are unified compactly to $\boldsymbol{P}, \boldsymbol{E} \succ \boldsymbol{0}$ and $\boldsymbol{B}' \succ \boldsymbol{0}$ with

$$4\underline{\lambda}(\boldsymbol{P})\underline{\lambda}(\boldsymbol{E}) \geq [\bar{\lambda}(\boldsymbol{B}') + |\varepsilon|\|\hat{\boldsymbol{C}}\|]^2.$$

In order to maximize the convergence rate α and region $\bar{\varrho}$, we thus in turn aim to maximize $\underline{\lambda}(\boldsymbol{P})$ and $\underline{\lambda}(\boldsymbol{E})$ while minimizing $\bar{\lambda}(\boldsymbol{B}')$ subject to $\underline{\lambda}(\boldsymbol{B}') > 0$. Therefore, we choose

$$\boldsymbol{\mathcal{K}} = \hat{\boldsymbol{\mathcal{K}}}_G + \kappa\boldsymbol{I} \tag{40}$$

Authorized licensed use limited to: TU Delft Library. Downloaded on July 10,2026 at 10:21:06 UTC from IEEE Xplore. Restrictions apply.

with constant $\kappa \in \mathbb{R}^+$ and split up (38) for $\eta_{\boldsymbol{e}} := \frac{\nu_{\boldsymbol{e}}}{\|\boldsymbol{e}\|^2}$ into

$$\mathbf{0} \preceq \underbrace{\begin{bmatrix} a\boldsymbol{I} & \frac{b}{2}\boldsymbol{I}-\varepsilon\alpha\hat{\boldsymbol{M}} \\ \frac{b}{2}\boldsymbol{I}-\varepsilon\alpha\hat{\boldsymbol{M}} & \gamma\boldsymbol{I}-(\varepsilon+\alpha)\hat{\boldsymbol{M}} \end{bmatrix}}_{=\boldsymbol{\Upsilon}(\alpha)} + \begin{bmatrix} \tilde{\boldsymbol{G}}+\varepsilon\eta_{\boldsymbol{e}}\boldsymbol{I} & \frac{\eta_{\boldsymbol{e}}+\varepsilon\eta_{\dot{\boldsymbol{e}}}}{2}\boldsymbol{I} \\ \frac{\eta_{\boldsymbol{e}}+\varepsilon\eta_{\dot{\boldsymbol{e}}}}{2}\boldsymbol{I} & \eta_{\dot{\boldsymbol{e}}}\boldsymbol{I} \end{bmatrix}$$
$$+ \underbrace{\begin{bmatrix} \varepsilon\tilde{\boldsymbol{K}}_P & \frac{1}{2}(\tilde{\boldsymbol{K}}_P+\varepsilon(\tilde{\boldsymbol{D}}-\hat{\boldsymbol{C}}^\top)) \\ \frac{1}{2}(\tilde{\boldsymbol{K}}_P+\varepsilon(\tilde{\boldsymbol{D}}-\hat{\boldsymbol{C}})) & \tilde{\boldsymbol{D}} \end{bmatrix}}_{=\boldsymbol{R}}$$
$$\tilde{\boldsymbol{G}} = \varepsilon\hat{\boldsymbol{K}}_G - \alpha\hat{\boldsymbol{\mathcal{K}}}_G,\ \tilde{\boldsymbol{K}}_P = \boldsymbol{K}_P - \underline{k}_P\boldsymbol{I},\ \tilde{\boldsymbol{D}} = \hat{\boldsymbol{D}}-\underline{\hat{d}}\boldsymbol{I}+\tilde{\boldsymbol{K}}_D. \tag{41}$$

Here, we have minimized $\boldsymbol{B}'$ and eliminated $-\frac{1}{2}\dot{\hat{\boldsymbol{\mathcal{K}}}}_G$ in $\boldsymbol{P}$ by cancelling $\hat{\boldsymbol{K}}_G$ and exploiting $\hat{G}(\boldsymbol{e}) = \frac{1}{2}\boldsymbol{e}^\top\hat{\boldsymbol{\mathcal{K}}}_G\boldsymbol{e}$ with

$$\dot{\hat{G}}(\boldsymbol{e}) = \dot{\boldsymbol{e}}^\top\hat{\boldsymbol{K}}_G\boldsymbol{e} \quad\Rightarrow\quad \frac{1}{2}\boldsymbol{e}^\top\dot{\hat{\boldsymbol{\mathcal{K}}}}_G\boldsymbol{e} = \dot{\boldsymbol{e}}^\top(\hat{\boldsymbol{K}}_G - \hat{\boldsymbol{\mathcal{K}}}_G)\boldsymbol{e}\,.$$

Also, we have directly made use of the obvious requirement $\varepsilon > 0$ for $\boldsymbol{P} \succ \mathbf{0}$ in (38) and introduced the constants

$$a = \varepsilon\left(\underline{k}_P - \frac{\vartheta}{2}\right) - \alpha\kappa,\ b = \underline{k}_P + \varepsilon(\underline{\hat{d}} + \underline{k}_D) - \kappa,$$
$$\gamma = \underline{\hat{d}} + \underline{k}_D - \frac{\varphi}{2}.$$

Note that, for the sake of simplicity, we refrain from an extended choice of $\boldsymbol{\mathcal{K}}$ enforcing $\boldsymbol{B}' = \mathbf{0}$ since it would involve additional matrix derivatives $\dot{\hat{\boldsymbol{D}}}, \dot{\hat{\boldsymbol{K}}}_{P,D}, (\dot{\eta}_{\boldsymbol{e}} + \varepsilon\dot{\eta}_{\dot{\boldsymbol{e}}})\boldsymbol{I}$. Therefore, we leverage Weyl's inequalities [37, Sect. III.2.1] next to transform (38) using the symmetric decomposition (41) to

$$\alpha\hat{G} \leq \underbrace{[\underline{\lambda}(\boldsymbol{\Upsilon}(\alpha)) + \underline{\lambda}(\boldsymbol{R})]}_{=\lambda(\alpha,t)}\|\boldsymbol{x}\|^2 + \varepsilon(\boldsymbol{e}^\top\hat{\boldsymbol{g}}_{\boldsymbol{e}} + \nu_{\boldsymbol{e}} + \omega_{\dot{\boldsymbol{e}}})$$
$$+ \nu_{\dot{\boldsymbol{e}}} + \omega_{\boldsymbol{e}} \tag{42}$$

with $\nu_{\boldsymbol{e}}$, $\nu_{\dot{\boldsymbol{e}}}$ and $\omega_{\boldsymbol{e}}$, $\omega_{\dot{\boldsymbol{e}}}$ from (22). Now, we exploit the commutability of the submatrices of $\boldsymbol{\Upsilon}$ in (41) to apply [42, Thm. 3] and follow for $\boldsymbol{v} = [a+\gamma-(\varepsilon+\alpha)\hat{\boldsymbol{m}}]/2$ that

$$\boldsymbol{\lambda}(\boldsymbol{\Upsilon}(\alpha)) = \boldsymbol{v}(\alpha) \pm \sqrt{\boldsymbol{v}^2(\alpha) + \left(\varepsilon\alpha\hat{\boldsymbol{m}} - \frac{b}{2}\right)^2 - a\,[\gamma-(\varepsilon+\alpha)\hat{\boldsymbol{m}}]}$$
$$= \boldsymbol{v}(\alpha) \pm \sqrt{\frac{[\gamma-a(\alpha)-(\varepsilon+\alpha)\hat{\boldsymbol{m}}]^2}{4} + \left(\varepsilon\alpha\hat{\boldsymbol{m}} - \frac{b}{2}\right)^2}. \tag{43}$$

To obtain an optimal parameterization, we consider

$$\max_{\kappa,\varphi\in\mathbb{R}^+} \underline{\lambda}(\boldsymbol{\Upsilon}) = \varepsilon\left(\underline{k}_P - \frac{\vartheta}{2}\right) - \alpha\kappa - \frac{(\varepsilon+\alpha)\Delta\hat{m}}{4}$$
$$\times\left(1 + \sqrt{1 + \frac{4\varepsilon^2\alpha^2}{(\varepsilon+\alpha)^2}}\right)$$

which then, subsequently, allows a maximal choice of convergence rate α such that (42) and thus (36) hold with equality. Here, we have directly reduced $\max\underline{\lambda}(\boldsymbol{\Upsilon})$ by optimally centering the two spheres generated by the spectrum of $\hat{\boldsymbol{M}}$ in the origin via the requirements $b = \varepsilon\alpha(\underline{\hat{m}} + \bar{\hat{m}})$ and $\gamma = a + (\varepsilon+\alpha)(\underline{\hat{m}} + \bar{\hat{m}})/2$, leading to the optimal parameters (25a) and (25b). Then, given values $\varepsilon, \vartheta \in \mathbb{R}^+$, obtained, e.g., via further numerical optimization based on the radius (37), we plug (43) into (42) and solve for the maximal α such that the resulting quadratic expression $0 \leq a_0 - 2a_1\alpha + a_2\alpha^2$ holds with equality. Finally, we obtain the time-variant rate $\alpha(t)$ as

$$\alpha(t) = \frac{1}{a_2(t)}\left(a_1(t) - \sqrt{a_1^2(t) - a_0(t)a_2(t)}\right) \tag{44}$$

with $a_{1-3}(t)$ given for $\hat{m}^*(t)$ s.t. $\underline{\lambda}(\boldsymbol{\Upsilon}(\alpha)) = \lambda^-(\boldsymbol{\Upsilon}(\hat{m}^*))$ by

$$a_0(t) = \xi^2(t) - \zeta^2(t) - b^2(t)$$
$$a_1(t) = \varkappa(t)\xi(t) + [\kappa - \hat{m}^*(t)]\zeta(t) - 2\varepsilon\hat{m}^*(t)b(t)$$
$$a_2(t) = \varkappa^2(t) - [\kappa - \hat{m}^*(t)]^2 - [2\varepsilon\hat{m}^*(t)]^2$$

where $\varkappa(t) = \kappa + \hat{m}^* + \frac{2\hat{G}(\boldsymbol{e})}{\|\boldsymbol{e}\|^2+\|\dot{\boldsymbol{e}}\|^2}$, $\zeta(t) = \gamma - \varepsilon(\underline{k}_P - \frac{\vartheta}{2} + \hat{m}^*)$, and

$$\xi(t) = \varepsilon\left(\underline{k}_P - \frac{\vartheta}{2} - \hat{m}^* + 2\frac{\boldsymbol{e}^\top\hat{\boldsymbol{g}}_{\boldsymbol{e}} + \nu_{\boldsymbol{e}} + \omega_{\dot{\boldsymbol{e}}}}{\|\boldsymbol{e}\|^2 + \|\dot{\boldsymbol{e}}\|^2}\right)$$
$$+ 2\left[\frac{\nu_{\dot{\boldsymbol{e}}} + \omega_{\boldsymbol{e}}}{\|\boldsymbol{e}\|^2 + \|\dot{\boldsymbol{e}}\|^2} + \underline{\lambda}(\boldsymbol{R})\right] + \gamma.$$

All together, exponential convergence and stability to within the ball $B(\varrho)$ from (23) can thus be concluded in the region

$$\boldsymbol{\mathcal{E}} = \Big\{\boldsymbol{e}, \dot{\boldsymbol{e}} \in \mathbb{R}^N \,\Big|\, \underline{\alpha}\hat{G}(\boldsymbol{e}) \leq [\underline{\lambda}(\boldsymbol{\Upsilon}) + \underline{\lambda}(\boldsymbol{R})](\|\boldsymbol{e}\|^2 + \|\dot{\boldsymbol{e}}\|^2)$$
$$+ \varepsilon(\boldsymbol{e}^\top\hat{\boldsymbol{g}}_{\boldsymbol{e}} + \nu_{\boldsymbol{e}} + \omega_{\dot{\boldsymbol{e}}}) + \nu_{\dot{\boldsymbol{e}}} + \omega_{\boldsymbol{e}}$$
$$\beta(\delta, d)\sqrt{\underline{\lambda}(\boldsymbol{\Sigma}_{\boldsymbol{\tau}}(t)) + s(d)} + Ld \leq \Delta\sqrt{\alpha(t)} \quad \forall t \geq t_0\Big\}$$

since (44) guarantees that (42) holds, and thus also (35) due to (36)–(41). ■

E. Design Interpretations

Intuitively, Lemma 2 provides a systematic approach to designing a Lyapunov function (or a contraction metric) for exponential stability proofs applied to Lagrangian systems. Typically, ε is chosen sufficiently small to ensure negative definiteness of the derivative, see, e.g., [33, p. 187], and eigenvalues are conservatively bounded, whereas we enable optimization of ε on the interval (26a) and provide exact expressions for the metric's spectrum in Corollary 1. Moreover, the results allow a systematic design of the stiffness $\boldsymbol{\mathcal{K}}$ contrary to the common approach only using the system's potential energy. In our case, we have employed the suboptimal choice (40) in sight of the analytical simplicity of the result, for which an optimal parametrization (25a) is then derived. Furthermore, we observe from (38) in the proof of Theorem 1 that setting $\boldsymbol{\mathcal{K}} = \boldsymbol{P}' + \varepsilon(\boldsymbol{E}' - 2\alpha\hat{\boldsymbol{M}})$ would maximize the spectrum of the considered matrix inequality on the right-hand side, and thus also the admissible convergence rate α.

The benefit of our structure-preserving control design is emphasized theoretically in Theorem 1. It is particularly visible

Authorized licensed use limited to: TU Delft Library. Downloaded on July 10,2026 at 10:21:06 UTC from IEEE Xplore. Restrictions apply.

in the influences on the exponential convergence rate in (42). Here, it becomes clear that the preservation of the potential energy (17a) and the conservative projector-based compensation (14)–(16), associated in (42) with the terms $\boldsymbol{e}^\top \hat{\boldsymbol{g}}_{\boldsymbol{e}}$ and $\nu_{\boldsymbol{e}} = h(\boldsymbol{e}^\top \hat{\boldsymbol{g}}_{\boldsymbol{q}})\boldsymbol{e}^\top \hat{\boldsymbol{g}}_{\boldsymbol{q}}$, $\nu_{\dot{\boldsymbol{e}}} = h(\dot{\boldsymbol{e}}^\top \hat{\boldsymbol{d}}_{\dot{\boldsymbol{q}}})\dot{\boldsymbol{e}}^\top \hat{\boldsymbol{d}}_{\dot{\boldsymbol{q}}}$, respectively, have a beneficial impact on the stability of the system. Moreover, the radius of the ball (23) clearly decreases with the term $\hat{G}(\boldsymbol{e})$ in (24) due to the structural preservation of the potential energy in the closed-loop system.

Also, note that a similar exponential stability result for the standard PD+ controller [22] can be derived using an ablation of the argumentation in Theorem 1. Then, the desired energy quantities become $\boldsymbol{g}_d(\boldsymbol{e}) = \boldsymbol{K}_P\boldsymbol{e}$ and $\boldsymbol{d}_d(\dot{\boldsymbol{e}}) = \boldsymbol{K}_D\dot{\boldsymbol{e}}$ with constant nonadaptive $\boldsymbol{K}_{P,D} \in \mathbb{R}^{N\times N}$, and friction as well as gravity are fully compensated. Therefore, we can conclude, based on our theoretical investigations, that the classical controller [22] is less robust due to the lower convergence rate and higher radius, stemming from the missing structural benefits since gravity and friction are fully compensated. This becomes particularly important for handling the possibly destabilizing effect of the Coriolis cross-term in (41) since $\boldsymbol{R}$ consists in the worst-case of a negative summand whose impact is scaled with $\|\hat{\boldsymbol{C}}\| \leq (\hat{c}_0 + \hat{c}_1\|\boldsymbol{q}\|)\|\dot{\boldsymbol{q}}\|$ with positive constants $\hat{c}_0, \hat{c}_1 \in \mathbb{R}^+$. Furthermore, the positive effect of the variance-based gain adaptation (18) can be seen by inspecting $\underline{\lambda}(\boldsymbol{R})$ from (41) and (42), since it has a direct influence on the convergence rate $\alpha(t)$, cf., e.g., (22), via $\lambda(\alpha, t) = \underline{\lambda}(\boldsymbol{\Upsilon}) + \underline{\lambda}(\boldsymbol{R})$. Reformulating $\boldsymbol{R}$ from (41) for $\tilde{\boldsymbol{K}}_P = \tilde{\boldsymbol{K}}_D$ to

$$\boldsymbol{R} = \underbrace{\begin{bmatrix} \varepsilon\tilde{\boldsymbol{K}}_P & \frac{1+\varepsilon}{2}\tilde{\boldsymbol{K}}_P \\ \frac{1+\varepsilon}{2}\tilde{\boldsymbol{K}}_P & \tilde{\boldsymbol{K}}_P \end{bmatrix}}_{=\tilde{\boldsymbol{K}}} + \underbrace{\begin{bmatrix} \boldsymbol{0} & \frac{\varepsilon}{2}\tilde{\boldsymbol{D}} \\ \frac{\varepsilon}{2}\tilde{\boldsymbol{D}} & \tilde{\boldsymbol{D}} \end{bmatrix}}_{=\tilde{\boldsymbol{\mathcal{D}}}} - \frac{\varepsilon}{2}\begin{bmatrix} \boldsymbol{0} & \hat{\boldsymbol{C}}^\top \\ \hat{\boldsymbol{C}} & \boldsymbol{0} \end{bmatrix}$$

we follow with Weyl's inequalities [37, Sect. III.2.1] that $\underline{\lambda}(\boldsymbol{R}) \geq \underline{\lambda}(\tilde{\boldsymbol{K}}) + \underline{\lambda}(\tilde{\boldsymbol{\mathcal{D}}}) - \frac{\varepsilon}{2}\|\hat{\boldsymbol{C}}\|$. Computing the spectrum

$$\boldsymbol{\lambda}(\tilde{\boldsymbol{K}}) = \frac{\boldsymbol{\lambda}(\tilde{\boldsymbol{K}}_P)}{2}\left(1 + \varepsilon \pm \sqrt{2(1+\varepsilon^2)}\right)$$

where we have applied [42, Thm. 3], we follow that $\underline{\lambda}(\tilde{\boldsymbol{K}}) \geq 0$ holds beneficially for $\varepsilon \geq 1$.

In the following numerical evaluations, we will validate these observations and even show that a classical PD+ controller can become unstable very early while our control law demonstrates a reliable performance despite increasing disturbance speeds.

V. Numerical Illustrations

In this section, we validate the efficacy of our proposed methods in numerical simulations.[1] At first, we start with a simple benchmark example for the sake of accessible interpretation and comparability and then move on to a higher system complexity illustrating scalable applicability along with practical feasibility.

[1] **Code:** For reproduction of our experiments, MATLAB code along with an L-GP toolbox [Online]. available: https://github.com/gevangelisti/lgp_prjctr_ctrl

A. Two-Link Manipulator

1) Setup: We benchmark our proposed control methods using the two-link robotic manipulator from [33, p. 164]. Gravity $g = 10$ m/s^2 acts along the positive x-axis as in [21] such that $\boldsymbol{q} = \boldsymbol{0}$ is an equilibrium of the system. The links are parametrized to have unit masses $m_n = 1$ kg and lengths $l_n = 1$ m for $n \in \{1, 2\}$. We additionally include dissipation via unit linear and quadratic damper elements at each joint, leading to $\boldsymbol{D}(\dot{\boldsymbol{q}}) = d_1\boldsymbol{I} + d_2\mathrm{diag}(|\dot{\boldsymbol{q}}|)$ with $d_1 = d_2 = 1$. The equations of motion are given by

$$\begin{bmatrix} \alpha + 2\beta\cos q_2 & \delta + \beta\cos q_2 \\ \delta + \beta\cos q_2 & \delta \end{bmatrix}\ddot{\boldsymbol{q}} + \begin{bmatrix} -\beta\dot{q}_2\sin q_2 & -\beta\sin q_2(\dot{q}_1 + \dot{q}_2) \\ \beta\dot{q}_1\sin q_2 & 0 \end{bmatrix}\dot{\boldsymbol{q}} + \boldsymbol{D}(\dot{\boldsymbol{q}})\dot{\boldsymbol{q}} + \begin{bmatrix} (m_1\frac{l_1}{2} + m_2 l_1)g\sin q_1 + m_2\frac{l_2}{2}g\sin(q_1+q_2) \\ m_2\frac{l_2}{2}g\sin(q_1+q_2) \end{bmatrix} = \boldsymbol{\tau}$$

where $\alpha = I_{z_1} + I_{z_2} + m_1\frac{l_1^2}{4} + m_2\left(l_1^2 + \frac{l_2^2}{4}\right)$, $\beta = m_2 l_1\frac{l_2}{2}$, $\delta = I_{z_2} + m_2\frac{l_2^2}{4}$, and $I_{z_n} = \frac{1}{3}m_n l_n^2$ for $n \in \{1, 2\}$. Parameter estimates are available but erroneous: $\hat{m}_n = (1+\chi_n)m_n$, $\hat{l}_n = (1+\chi_n)l_n$ and $\hat{d}_n = (1-\chi_n)d_n$ with an alternating relative bias of 50% such that $\chi_n = (-1)^{n-1/2}$.

2) Training: For the L-GP's hyperparameters, we use $D = 5^2 + 3^2$ training and $V = 6^2$ validation data pairs stemming from equally distanced grids on the domains $\boldsymbol{q} \in [-a, a]^2$ for $a = 1, 1.25$ with fixed velocity $\dot{\boldsymbol{q}} = [-1, 1]^\top, [1.5, 0]^\top$ and acceleration $\ddot{\boldsymbol{q}} = \boldsymbol{4}, \boldsymbol{0}$, respectively. Due to the additional dissipative subcomponent, the training dataset also includes a small 3×3 grid in the velocity domain $\dot{\boldsymbol{q}} \in [-1, 1]^2$ for $\boldsymbol{q} = \ddot{\boldsymbol{q}} = \boldsymbol{0}$. Torque and acceleration measurements are corrupted by independent identically distributed noise with standard deviations of 0.1 Nm and $\pi/180$ rad/s^2, respectively. We reduce the kinetic mass inertia hypermetric to the constant Euclidian form $\boldsymbol{\Lambda}^{-1} = \sigma_{\boldsymbol{d}_T}^2\boldsymbol{I}$. Similarly, we assume a gravitational distance covariance $\boldsymbol{\Sigma}_{\boldsymbol{d}_G} = \mathrm{diag}(\boldsymbol{\sigma}_{\boldsymbol{d}_G}^2)$. The hyperparameters are then optimized via the least-squares approximation of all $D + V = 70$ measurements.

3) Control: As a control task, we first consider the goal of tracking an eight-curve figure, cf., Fig. 2, starting from the initial condition $\boldsymbol{q}(0) = \pi/4\boldsymbol{1}$ and $\dot{\boldsymbol{q}}(0) = \boldsymbol{0}$. In addition to our proposed structure-preserving and L-GP-based controllers, we also compare with the standard parameteric ablation (PD+) from [33, p. 194] along with its L-GP extended counterpart (L-GP-PD+). To prevent numerical stability issues, we implement the projection matrices as

$$\boldsymbol{P}_{\boldsymbol{e}} = \frac{\boldsymbol{e}\boldsymbol{e}^\top}{\epsilon + \|\boldsymbol{e}\|^2} \tag{45}$$

with an $\epsilon = 10^{-3}$. Note that this is a common numerical procedure often employed in other inversion implementations, such as, e.g., mass matrix predictions with DeLaNs [6] or Cholesky

Authorized licensed use limited to: TU Delft Library. Downloaded on July 10,2026 at 10:21:06 UTC from IEEE Xplore. Restrictions apply.

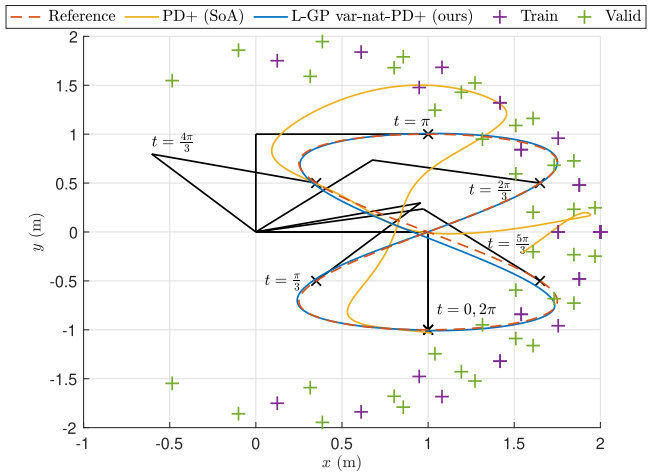


Fig. 2. Reference trajectory in the cartesian workspace of the two-link for $t \in 6n\pi + [0, 2\pi]$, $n \in \mathbb{N}_0$ and tracking performance comparison of the standard parameteric PD+ with the proposed variance-adaptive and structure-preserving, L-GP-based, PD+ controller.

TABLE I
NUMERICAL EVALUATION OF THE STEADY-STATE CONTROLLER PERFORMANCES FOR $t \geq 10$S BASED ON THE TWO-LINK

	PD+ (SoA)	L-GP-PD+ (new)	nat-PD+ (ours)	L-GP nat-PD+ (ours)	L-GP var-nat-PD+ (ours)
$\|\boldsymbol{\tau}\|_{\mathcal{L}_2}$	33.49	27.95	27.86	24.40	**24.09**
$\max(\|\boldsymbol{\tau}\|)$	25.79	19.73	26.52	18.19	**15.92**
$\mathrm{E}[\|\boldsymbol{\tau}\|]$	9.635	7.946	7.798	7.085	**7.014**
$\|[\boldsymbol{e}^\top \dot{\boldsymbol{e}}^\top]\|_{\mathcal{L}_2}$	1.798	0.983	0.970	0.838	**0.129**
$\max(\|\boldsymbol{e}\|)$	0.619	0.352	0.257	0.308	**0.043**
$\max(\|\dot{\boldsymbol{e}}\|)$	0.967	0.807	0.995	0.735	**0.093**
$\mathrm{E}[\|\boldsymbol{e}\|]$	0.379	0.112	0.133	0.106	**0.020**
$\mathrm{E}[\|\dot{\boldsymbol{e}}\|]$	0.376	0.243	0.214	0.176	**0.031**

Winning method's value is printed bold per metric.

decompositions of covariance matrices [26]. Moreover, all controllers are parametrized by the same proportional and derivative corrections $\boldsymbol{K}_P = \boldsymbol{K}_D = 10\boldsymbol{I}$. The variance-adaptive natural PD+ controller (L-GP var-nat-PD+) additionally uses the gains (18), which are identically set to $\boldsymbol{K}_i = k_i \boldsymbol{I}$ with $k_1 = 10^2$, $k_2 = 0.02$, and $k_3 = 7.11$ such that $\underline{k}_P = \underline{k}_D = 10 + 1$. Note that instead of assuming their measurability, the accelerations required to compute the L-GP covariance are estimated based on the model.

4) Results: The simulation results are illustrated in Fig. 3 and the steady-state performances evaluated numerically in Table I. Despite considerable errors in the parameters, the proposed natural PD+ controller (nat-PD+) already shows significantly improved error metrics, demonstrating its natural robustness due to the preservation of the system's physical structure. Furthermore, employing the mean estimate of the L-GP greatly improves the tracking accuracy of both standard (L-GP-PD+) and natural (L-GP nat-PD+) controllers. Intuition for the functioning of the structure-preserving controllers can be gained by inspecting Fig. 3 for small transient times close to zero. Here, both variants without uncertainty-adaptation start with considerably lower actuation efforts due to the exploited system structures. The uncertainty-based adaptation law (L-GP var-nat-PD+), variably shaping and injecting potential energy and damping, respectively, demonstrates the highest tracking accuracy w.r.t. all error metrics while having to actuate with the lowest effort based on the torque input's $\mathcal{L}_2$-norm. Its slightly increased mean over time hints at the tradeoff between actuation and accuracy performed by the uncertainty-dependent feedback gains.

For the validation of Theorem 1, we first evaluate the proposed Lyapunov function (30) and its bounds (28) in Fig. 4 based on the metric (27) from Lemma 2 with the design stiffness (40) for different closed-loop trajectories of the L-GP-based natural PD+ controller (L-GP nat-PD+). For generality, we now consider a sinusoidal reference trajectory $\boldsymbol{q}_d(t) = \pi/2 \sin(t)\mathbf{1}$ from here onward. Initial conditions are randomly drawn from $\boldsymbol{q}(0) \sim \mathcal{N}(\mathbf{0}, \sigma_0^2 \boldsymbol{I})$ and $\dot{\boldsymbol{q}}(0) \sim \mathcal{N}(\pi/2 \cdot \mathbf{1}, \sigma_0^2 \boldsymbol{I})$ with a standard deviation of $\sigma_0 = \pi/3$. Then, we compute the norm of the simulated trajectory errors and validate that the exponential convergence bound (21) holds for all realizations and times $t \geq 0$. Here, we have used the parameter values $\varepsilon = 1.1012$ and $\vartheta = 1.4211$ and minimal convergence rate $\underline{\alpha} = 0.1056$, which were obtained by solving

$$\min_{\varepsilon, \vartheta, \underline{\alpha}} \underline{\varrho}(\varepsilon, \vartheta) + \frac{1}{\underline{\alpha}} \quad \text{s.t.} \quad \kappa, \varphi > 0, \sqrt{\frac{\kappa}{\hat{m}}} > \varepsilon > 0, \underline{\lambda}(\boldsymbol{\Upsilon}(\underline{\alpha})) \geq \underline{\upsilon}$$

numerically for $\underline{\upsilon} = 6$ with the virtual stiffness $\kappa = 21.12$ and scale $\varphi = 0.3658$ following from (25a) and (25b) and the worst-case radius $\underline{\varrho}$ from (23) for $\Delta = 0.5269$. The time evolution of convergence rate and ball radius is illustrated in Fig. 5 for the same L-GP nat-PD+ trajectories along with the variance-adaptive extension. The latter clearly shows an improved convergence behavior for the same initial conditions.

Finally, in order to confirm the overall performance increase of the proposed structural preserving and variance-adaptive controllers, we perform a Monte Carlo simulation over the initial conditions and frequency ω of the sinusoidal reference $\boldsymbol{q}_d(t) = \pi/2 \sin(\omega t)\mathbf{1}$. Therefore, we simulate 100 realizations per frequency sample, where the initial conditions of the two-link are drawn from a uniform distribution over $\boldsymbol{q}, \dot{\boldsymbol{q}} \in [-a, a]^4$ for $a = \pi/4$. The results in Fig. 6 show the $\mathcal{L}_2$-norms of the error state vector and actuation over the frequency ω, evaluated in the steady-state for $t \geq 4\pi/\omega$. Not only can we validate subsequent increases in the tracking accuracy, but we can also observe the superior robustness of the proposed controllers. Despite rising disturbance speeds, the natural PD+ controllers structurally ensure stability and, thus, a reliable performance, whereas the standard PD+ versions become unstable regardless of the used parameteric or L-GP-based model.

B. Planar Soft Robot

1) Setup: Next, we consider the planar soft robot from [17] and [43], simulated by a finite element method (FEM)-based model. For this, we employ a discretization of a continuous rod with unit mass and length as a series of infinitesimal links [44], where we consider a total of $N_{\text{FEM}} = 100$ with lumped rotational principle inertias of $I_n = 1/(12N_{\text{FEM}}^3)$, $n \in \{1, \ldots, 100\}$, each subsequently connected by linear torsional–spring–damper elements. These stiffnesses and dampings are set to $k_n = 10$ Nm rad^{-1} and $d_n = 5$ Nm rad s^{-1}, respectively.

Authorized licensed use limited to: TU Delft Library. Downloaded on July 10,2026 at 10:21:06 UTC from IEEE Xplore. Restrictions apply.

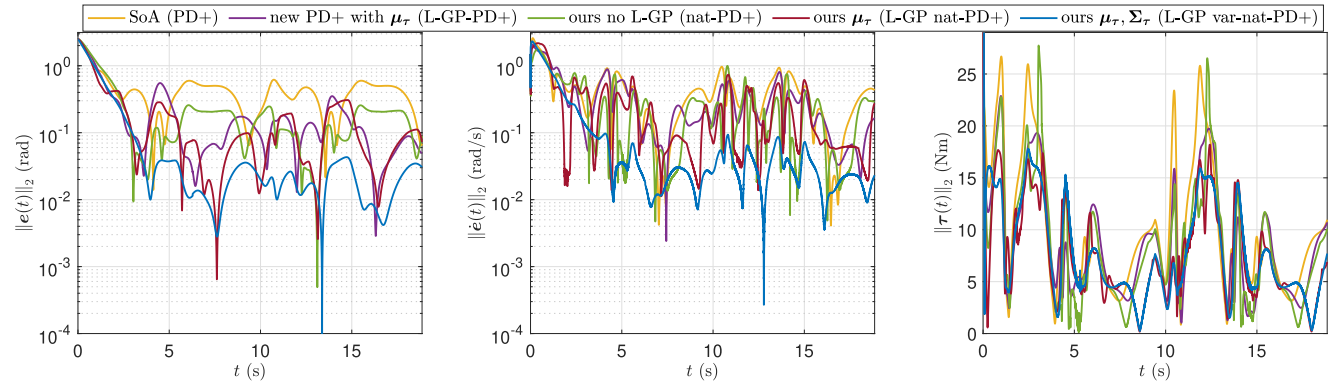


Fig. 3. Tracking performances of the standard parameteric and proposed, structure-preserving or L-GP-based, PD+ controllers. The left/middle and right subplots show the norms of the position/velocity error and the actuation vectors, respectively.

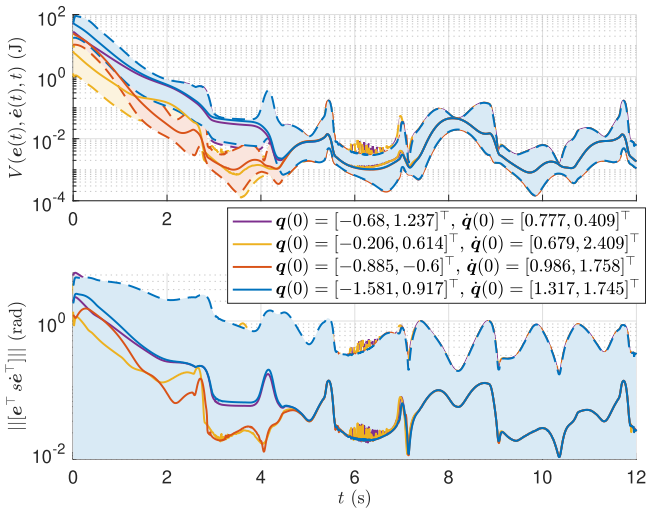


Fig. 4. L-GP nat-PD+ controller: Lyapunov function and bounds for trajectories with different initial conditions $q_0 \sim \mathcal{N}(\mathbf{0}, \sigma_0^2 \boldsymbol{I})$ and $\dot{q}_0 \sim \mathcal{N}(\pi/2 \cdot \mathbf{1}, \sigma_0^2 \boldsymbol{I})$, where $\sigma_0 = \pi/3$. Solid lines indicate trajectories, shaded areas respective functional or error norm regions from Theorem 1 and Lemma 2 with the bounds (21) and (28) given by the dashed lines.

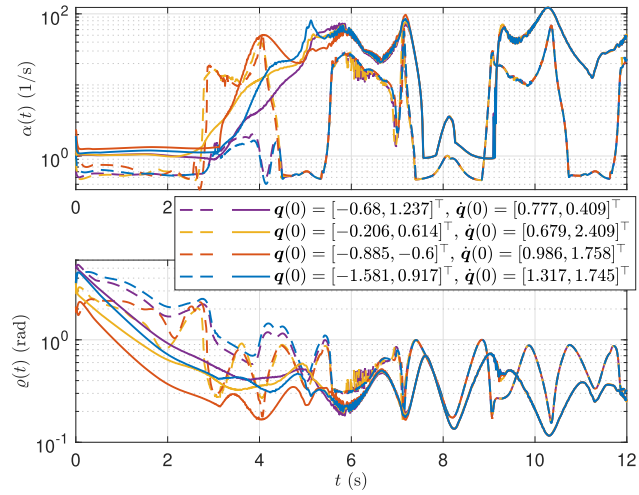


Fig. 5. Exponential convergence behaviors of the proposed natural structure-preserving controllers evaluated on the two-link for randomly drawn initial conditions, as shown in Fig. 4. Solid lines indicate the variance-adaptive (L-GP var-nat-PD+) controller, dashed the static gain (L-GP nat-PD+) variant.

The FEM simulation is implemented in MATLAB based on the articulated body algorithm from [45]. As shown in Section V-A and [17], we rotate the base frame such that the soft arm is aligned with gravity in its equilibrium $\boldsymbol{q}^{\text{FEM}} = \mathbf{0}$ with $\boldsymbol{q}^{\text{FEM}} \in \mathbb{R}^{N_{\text{FEM}}}$.

2) Training: For training, we consider the system's step response to a constant torque with amplitude $a = 1$ Nm continuously acting on each FEM element, starting from equilibrium. The L-GP uses $D = 24$ equidistant samples, corrupted by measurement noise with standard deviation $0.01a$, of the simulated trajectory for $0 \leq t \leq 4$ s, while discretizing into $N = 4$ constant curvature (CC) segments [17] equivalent to a constrained rigid body with $4N = 16$ DOFs. For the parameters, estimates $\hat{m}_n = (1 + \chi_n)/N$, $\hat{k}_n = k_n N(1 + \chi_n)/N_{\text{FEM}}$, and $\hat{d}_n = d_n N/N_{\text{FEM}}$ are used for the masses, stiffnesses, and dampings, respectively, with relative errors $\chi_n = (-1)^{n-1}/4$ for $n \in \{1, 2, 3, 4\}$. We reduce to Euclidian inertial and diagonal gravitational hypermetrics analogously to Section V-A. In addition, we exploit symmetries of the robot's configuration by asserting symmetric [46] squared-exponential kernels for kinetic and potential energies, leading for the latter to a point-symmetric restoring potential force $\hat{g}(-\boldsymbol{q}) = -\hat{g}(\boldsymbol{q})$. Then, the hyperparameters are optimized based on the least-squares approximation of the FEM positions with the L-GP-based dynamical resimulation, where we consider a sampling frequency of 250 Hz leading to $V = 1001$ validating position samples of the training trajectory.

3) Control: The standard and proposed, natural structure-preserving or L-GP-based, controllers with identical proportional and derivative gains $\boldsymbol{K}_P = \boldsymbol{K}_D = \boldsymbol{I}$ are tasked with tracking a sinusoidal reference $\boldsymbol{q}_d(t) = \bar{\boldsymbol{a}} \sin t$ with amplitude vector $\bar{\boldsymbol{a}} = \pi/180[1, 10, 45, 90]$ in the considered 8-D CC state space, cf., Fig. 7. The system is initially assumed to be at rest, $\dot{\boldsymbol{q}}(0) = \mathbf{0}$, but deflected by the maximum amplitude $\boldsymbol{q}(0) = -\bar{\boldsymbol{a}}$. Projectors of the structure-preserving controllers are implemented again with the same $\epsilon = 10^{-3}$, as in (45). The

Authorized licensed use limited to: TU Delft Library. Downloaded on July 10,2026 at 10:21:06 UTC from IEEE Xplore. Restrictions apply.

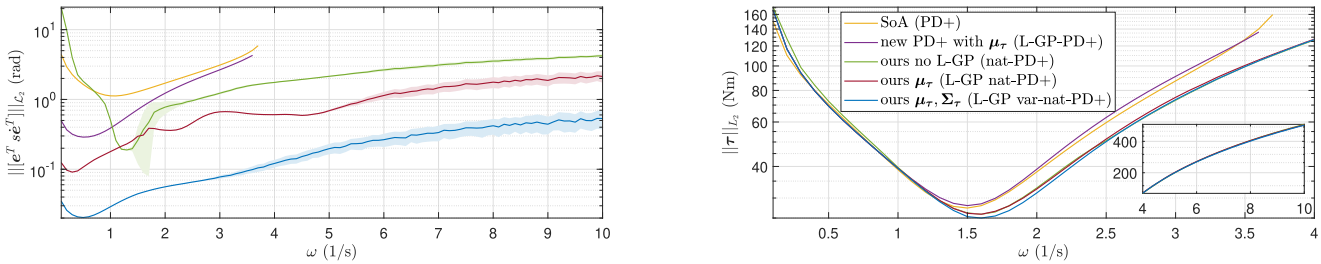


Fig. 6. Monte Carlo evaluation of the standard parameteric and the proposed, natural structure-preserving or L-GP-based, PD+ controllers. Solid lines and shaded areas depict respective mean and standard deviation of 100 realizations per frequency sample. Initial conditions are randomly drawn from the uniform distribution over $[\boldsymbol{q}_0^\top \dot{\boldsymbol{q}}_0^\top] \in [-\pi/4, \pi/4]^4$. Both standard PD+ controllers with full gravity cancellation become unstable at 3.7 and 3.8 rad s^{-1}.

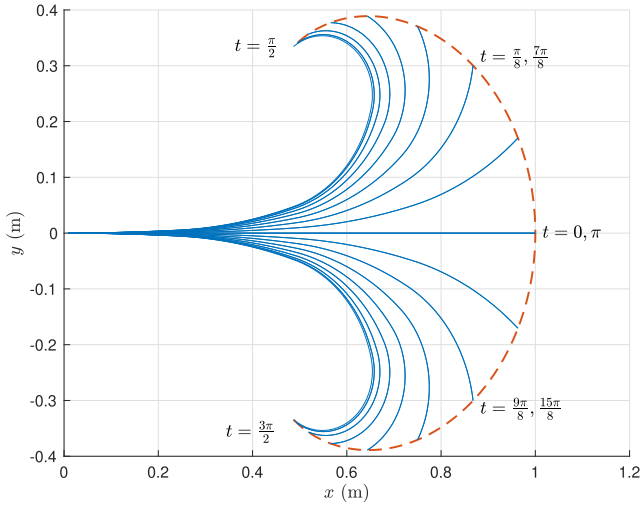


Fig. 7. Reference trajectory of the soft robot moving in its planar workspace.

TABLE II
NUMERICAL EVALUATION OF THE STEADY-STATE CONTROL PERFORMANCES FOR $t \geq 2\pi$S BASED ON THE SOFT ROBOT

	PD+ (SoA)	L-GP-PD+ (new)	nat-PD+ (ours)	L-GP nat-PD+ (ours)	L-GP var-nat-PD+ (ours)
$\|\boldsymbol{\tau}\|_{\mathcal{L}_2}$	**5.00**	5.24	5.32	5.45	5.46
$\max(\|\boldsymbol{\tau}\|)$	**1.89**	1.96	1.99	2.04	2.05
$\mathrm{E}[\|\boldsymbol{\tau}\|]$	**1.313**	1.395	1.408	1.436	1.439
$\|\|[\boldsymbol{e}^\top \dot{\boldsymbol{e}}^\top]\|\|_{\mathcal{L}_2}$	0.670	0.379	0.650	0.059	**0.042**
$\max(\|\boldsymbol{e}\|)$	0.191	0.116	0.185	0.013	**0.010**
$\max(\|\dot{\boldsymbol{e}}\|)$	0.181	0.089	0.210	0.022	**0.017**
$\mathrm{E}[\|\boldsymbol{e}\|]$	0.123	0.088	0.118	0.008	**0.005**
$\mathrm{E}[\|\dot{\boldsymbol{e}}\|]$	0.125	0.057	0.113	0.0135	**0.0099**

Lower values indicate better performances w.r.t. the considered metrics.

covariance gains (18) of the adaptive natural PD+ controller are identically set to diagonal $\boldsymbol{K}_i = k_i \boldsymbol{I}$ with $k_1 = 10$, $k_2 = 10^{-3}$, and $k_3 = 10.05$ such that $\underline{k}_P = \underline{k}_D = 1 + 0.1$. Also, instead of assuming their direct measurability, model-based estimates of the accelerations are used to compute the L-GP covariance.

4) Results: The controllers' tracking performances are visualized in Fig. 8, and their steady-state accuracies are evaluated numerically in Table II. Aside from the significant performance increases achieved by the application of the L-GP model, the natural structure-preserving (L-GP nat-PD+) controller also leads to another drastic improvement by a factor of 6.47 compared to the standard (L-GP-)PD+ variant w.r.t. the $\mathcal{L}_2$-norm of the trajectory error. The proposed variance-adaptive (L-GP var-nat-PD+) controller demonstrates the highest tracking accuracy w.r.t. all error metrics with slightly increased actuation effort, however.

Next, we apply Theorem 1 to compare the convergence and reliability of the controllers tracking the soft robot's reference curvature. The according Lyapunov functions (30) and their bounds (28) are evaluated in Fig. 9, where the gravitational energy $\hat{G}(\boldsymbol{e}) = \frac{1}{2}\boldsymbol{e}^\top \hat{\boldsymbol{\mathcal{K}}}_G(\boldsymbol{e})\boldsymbol{e}$ is eliminated from the metric (27) with design stiffness (40) for the standard PD+ controller due to its cancellation. The norms of the closed-loop errors and the exponential convergence bounds (21) are shown in the middle subplot of Fig. 9, confirming their validity for each of the controllers $\forall t \geq 0$ and also demonstrating their applicability to higher system dimensionalities. As shown in Section V-A4, we optimally parametrize all guarantees by leveraging (25a) and (25b) and numerical minimization of the worst-case radius $\underline{\varrho}$ from (23), for an L-GP model error bound of $\Delta = 0.9556$. The resulting time evolutions of convergence rate $\alpha(t)$ and ball radius $\varrho(t)$ of all L-GP-based controllers are visualized in the bottom and middle subplots of Fig. 9 by the solid and dashed lines, respectively. Compared to the standard (L-GP-)PD+, the structure-preserving (L-GP nat-PD+) controller without variance adaptation already leads to significantly increased reliability and convergence with an improved exponential rate and radius by up to two and three orders of magnitude, respectively. Finally, the variance-adaptive (L-GP var-nat-PD+) version shows the best behavior, with a big improvement compared to the static-gain (L-GP nat-PD+) counterpart, particularly visible in the transient phase $0 \leq t \leq 5$ s.

VI. CONCLUSION

We have proposed a structure-preserving tracking controller using projections and a learned model given by the posterior of an L-GP. The uncertainty quantification in the form of the covariance matrix is encoded into a confidence-dependent feedforward-feedback balancing scheme. High accuracy and performance are guaranteed by precise theoretical results, ensuring exponential convergence and stability probabilistically.

Authorized licensed use limited to: TU Delft Library. Downloaded on July 10,2026 at 10:21:06 UTC from IEEE Xplore. Restrictions apply.

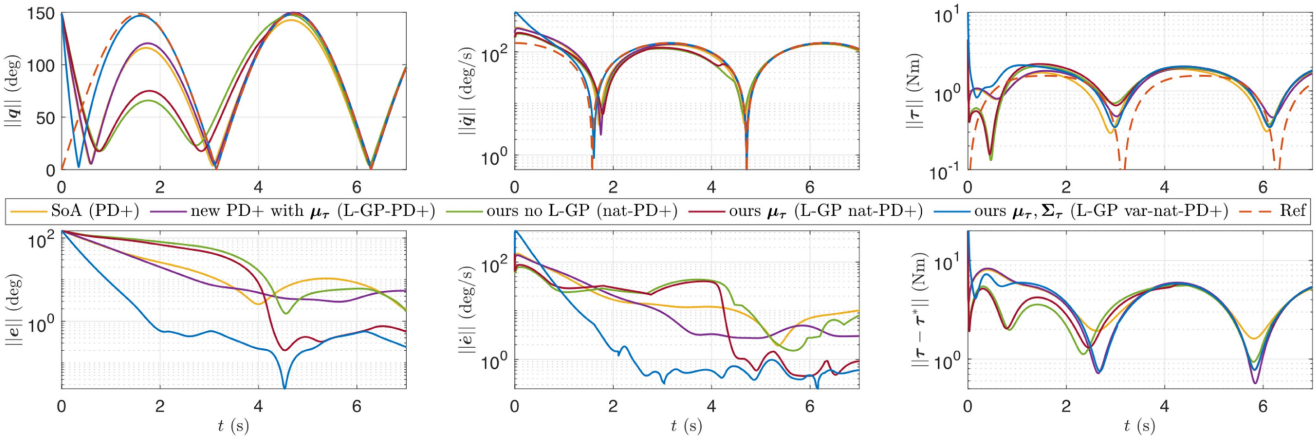


Fig. 8. Tracking performances of the standard parameteric and proposed, natural structure-preserving or L-GP-based, PD+ controllers in the N-dimensional curvature space of the soft robot, $N = 4$, for the initial condition $\boldsymbol{q}(0) = -\bar{\boldsymbol{a}}$, $\dot{\boldsymbol{q}}(0) = \mathbf{0}$. The reference torque $\boldsymbol{\tau}^*(t)$ indicates the nominal (feedforward) actuation based on the FEM for zero tracking errors.

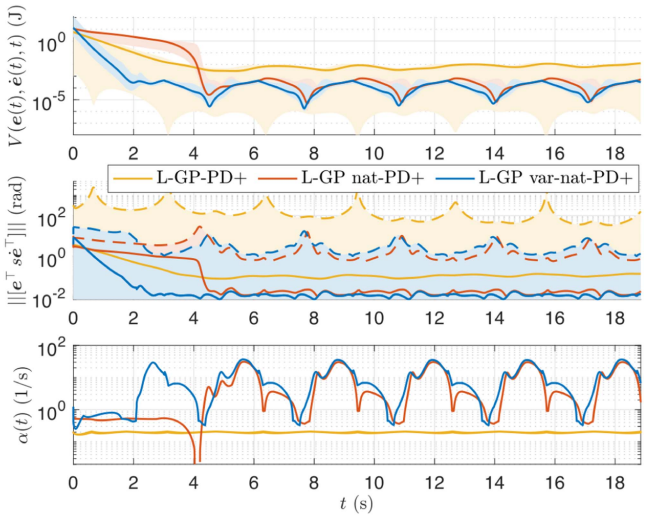


Fig. 9. Lyapunov functions, bounds, and exponential convergence rates of all L-GP-based controllers for the closed-loop trajectories from Fig. 8. Solid lines indicate trajectories, shaded areas functional (28), or error norm (21) bounds from Lemma 2 or Theorem 1, respectively.

Numerical simulations of robotic systems, a planar two-link, and soft manipulator, confirm the theoretical and practical efficacy of the proposed methods.

Appendix I
Supplementary Proofs

A. Proof of Lemma 2

Using Schur complements [41], the equivalence

$$\boldsymbol{\mathcal{M}} \succ \mathbf{0} \quad \Leftrightarrow \quad \boldsymbol{\mathcal{K}} - \varepsilon^2 \hat{\boldsymbol{M}} \hat{\boldsymbol{M}}^{-1} \hat{\boldsymbol{M}} \succ \mathbf{0}$$

can be used to follow that $\varepsilon^2 \hat{\boldsymbol{M}} \prec \boldsymbol{\mathcal{K}}$ must hold for positive definiteness of $\boldsymbol{\mathcal{M}}$, since $\hat{\boldsymbol{M}} \succ \mathbf{0}$. Then, applying Weyl's inequalities [37, Sect. III.2.1], we arrive at $\varepsilon^2 \bar{\hat{m}} < \underline{\kappa}$. Taking the square root and reformulating leads to the first condition. Next, for the proof of (28), we start off with the nonstrict LMIs

$$\mathbf{0} \preceq \boldsymbol{\mathcal{M}} - \underline{\mu} \boldsymbol{I}, \quad \mathbf{0} \preceq \bar{\mu} \boldsymbol{I} - \boldsymbol{\mathcal{M}}.$$

Given $\hat{\boldsymbol{M}} \neq \boldsymbol{\mathcal{K}}$, we can always find positive values satisfying $\underline{\mu} < \max(\underline{\kappa}, \underline{\hat{m}})$ and $\bar{\mu} > \min(\bar{\kappa}, \bar{\hat{m}})$ such that either $\boldsymbol{\mathcal{K}} - \underline{\mu} \boldsymbol{I}, \bar{\mu} \boldsymbol{I} - \boldsymbol{\mathcal{K}} \succ \mathbf{0}$ or $\hat{\boldsymbol{M}} - \underline{\mu} \boldsymbol{I}, \bar{\mu} \boldsymbol{I} - \hat{\boldsymbol{M}} \succ \mathbf{0}$ hold, respectively. Thus, we analogously apply Schur complements and Weyl's inequalities, leading to the quadratic inequalities $\underline{\mu}^2 - (\underline{\kappa} + \underline{\hat{m}})\underline{\mu} + \underline{\hat{m}}\underline{\kappa} - \varepsilon^2 \bar{\hat{m}}^2 \geq 0$. Solving for $\underline{\mu}$, we obtain (28b). Choosing the upper and lower zero crossings for the upper and lower bounding values $\bar{\mu}$ and $\underline{\mu}$ then guarantees that $\max(\bar{\kappa}, \bar{\hat{m}}) < \bar{\mu}$ and $0 < \underline{\mu} < \min(\underline{\kappa}, \underline{\hat{m}})$ hold, respectively, for $0 < |\varepsilon| < \sqrt{\underline{\hat{m}}\underline{\kappa}}/\bar{\hat{m}}$. Finally, let us consider the special case of $\hat{\boldsymbol{M}} = \boldsymbol{\mathcal{K}}$. Then, we can directly compute the eigenvalues of (27) analytically using its characteristic polynomial

$$\begin{aligned} \hat{\boldsymbol{M}} = \boldsymbol{\mathcal{K}} \;\Rightarrow\; & \det(\boldsymbol{\mathcal{M}} - \lambda \boldsymbol{I}) \\ & = \det[(\hat{\boldsymbol{M}} - \lambda \boldsymbol{I})^2 - (\varepsilon \hat{\boldsymbol{M}})^2] \\ & = \det[(1-\varepsilon)\hat{\boldsymbol{M}} - \lambda \boldsymbol{I}] \det[(1+\varepsilon)\hat{\boldsymbol{M}} - \lambda \boldsymbol{I}] \end{aligned}$$

where we have applied the formula for determinants of 2×2 block matrices [42, Thm. 3] in the second line, valid since $\varepsilon \hat{\boldsymbol{M}}$ and $\hat{\boldsymbol{M}} - \lambda \boldsymbol{I}$ commute, along with the multiplicativity property of the determinant in the last line. In this case, the spectrum of $\boldsymbol{\lambda}(\boldsymbol{\mathcal{M}})$ is therefore the result of the eigenvalues $\boldsymbol{\lambda}(\hat{\boldsymbol{M}})$ being scaled by $1 \pm \varepsilon$, such that $\boldsymbol{\lambda}(\boldsymbol{\mathcal{M}}) = (1 \pm \varepsilon)\boldsymbol{\lambda}(\hat{\boldsymbol{M}})$ holds. Clearly, this coincides with $\underline{\mu} = \underline{\lambda}(\boldsymbol{\mathcal{M}})$ in (28b) for $\underline{\kappa} = \underline{\hat{m}}$, and positive definiteness necessarily requires $|\varepsilon| < 1$, which is encompassed by the second (sufficient) condition of the lemma on $|\varepsilon|$ since $\underline{\hat{m}}/\bar{\hat{m}} \leq 1$.

B. Proof of Corollary 1

Using the commutability of $\varepsilon \hat{\boldsymbol{M}}$ and $\hat{\boldsymbol{M}} - \lambda \boldsymbol{I}$ combined with [42, Thm. 3], we can compute the characteristic polynomial of (27) according to

$$\boldsymbol{\mathcal{K}} = \kappa \boldsymbol{I} \;\Rightarrow\; \det(\boldsymbol{\mathcal{M}} - \lambda \boldsymbol{I})$$

Authorized licensed use limited to: TU Delft Library. Downloaded on July 10,2026 at 10:21:06 UTC from IEEE Xplore. Restrictions apply.

$$= \det[(\boldsymbol{\mathcal{K}} - \lambda \boldsymbol{I})(\hat{\boldsymbol{M}} - \lambda \boldsymbol{I}) - \varepsilon^2 \hat{\boldsymbol{M}}^2]$$

$$= \det[\underbrace{(\kappa - \lambda)\hat{\boldsymbol{M}} - \varepsilon^2 \hat{\boldsymbol{M}}^2}_{:=\hat{\boldsymbol{A}}} - \lambda(\kappa - \lambda)\boldsymbol{I}].$$

Thus, $\det(\boldsymbol{\mathcal{M}} - \lambda \boldsymbol{I}) = 0$ holds iff $\lambda(\kappa - \lambda)$ is an eigenvalue of $\hat{\boldsymbol{A}}$, leading for $\hat{\mu} := \lambda(\hat{\boldsymbol{M}})$ to the algebraic condition

$$(\kappa - \lambda)\hat{\mu} - \varepsilon^2 \hat{\mu}^2 = \lambda(\kappa - \lambda) \tag{46}$$

where we have used $\boldsymbol{A}^2 \boldsymbol{x} = \lambda^2(\boldsymbol{A})\boldsymbol{x}$ for $\boldsymbol{A} \in \mathbb{R}^{N \times N}$. Finally, solving the quadratic (46) for the desired eigenvalues $\lambda \equiv \lambda(\boldsymbol{\mathcal{M}})$ and vectorizing, we arrive at (29).

REFERENCES

[1] G. Evangelisti and S. Hirche, "Data-driven momentum observers with physically consistent Gaussian processes," *IEEE Trans. Robot.*, vol. 40, pp. 1938–1951, 2024.

[2] A. R. Geist and S. Trimpe, "Structured learning of rigid-body dynamics: A survey and unified view from a robotics perspective," *GAMM-Mitteilungen*, vol. 44, no. 2, 2021, Art. no. e202100009.

[3] K. Rath, C. G. Albert, B. Bischl, and U. von Toussaint, "Symplectic Gaussian process regression of maps in Hamiltonian systems," *Chaos: An Interdiscipl. J. Nonlinear Sci.*, vol. 31, no. 5, 2021, Art. no. 053121.

[4] S. Ober-Blöbaum and C. Offen, "Variational learning of Euler–Lagrange dynamics from data," *J. Comput. Appl. Math.*, vol. 421, 2023, Art. no. 114780.

[5] G. Giacomuzzo, R. Carli, D. Romeres, and A. Dalla Libera, "A black-box physics-informed estimator based on Gaussian process regression for robot inverse dynamics identification," *IEEE Trans. Robot.*, vol. 40, pp. 4820–4836, 2024.

[6] M. Lutter and J. Peters, "Combining physics and deep learning to learn continuous-time dynamics models," *Int. J. Robot. Res.*, vol. 42, no. 3, pp. 83–107, 2023, doi: 10.1177/02783649231169492.

[7] M. Lutter, K. Listmann, and J. Peters, "Deep Lagrangian networks for end-to-end learning of energy-based control for under-actuated systems," in *Proc. IEEE/RSJ Int. Conf. Intell. Robots Syst.*, 2019, pp. 7718–7725.

[8] M. W. Spong, "Energy based control of a class of underactuated mechanical systems," *IFAC Proc. Volumes*, vol. 29, no. 1, pp. 2828–2832, 1996. [Online]. Available: https://www.sciencedirect.com/science/article/pii/S1474667017581057

[9] D. Nguyen-Tuong and J. Peters, "Local Gaussian process regression for real-time model-based robot control," in *Proc. IEEE/RSJ Int. Conf. Intell. Robots Syst.*, 2008, pp. 380–385.

[10] J. F. Fisac, A. K. Akametalu, M. N. Zeilinger, S. Kaynama, J. Gillula, and C. J. Tomlin, "A general safety framework for learning-based control in uncertain robotic systems," *IEEE Trans. Autom. Control*, vol. 64, no. 7, pp. 2737–2752, Jul. 2019.

[11] T. Beckers, D. Kulić, and S. Hirche, "Stable Gaussian process based tracking control of Euler–Lagrange systems," *Automatica*, vol. 103, pp. 390–397, 2019.

[12] J. Umlauft and S. Hirche, "Feedback linearization based on Gaussian processes with event-triggered online learning," *IEEE Trans. Autom. Control*, vol. 65, no. 10, pp. 4154–4169, Oct. 2020.

[13] L. Hewing, J. Kabzan, and M. N. Zeilinger, "Cautious model predictive control using Gaussian process regression," *IEEE Trans. Control Syst. Technol.*, vol. 28, no. 6, pp. 2736–2743, Nov. 2020.

[14] J. Berberich, J. Köhler, M. A. Müller, and F. Allgöwer, "Data-driven model predictive control with stability and robustness guarantees," *IEEE Trans. Autom. Control*, vol. 66, no. 4, pp. 1702–1717, Apr. 2021.

[15] M. Maiworm, D. Limon, and R. Findeisen, "Online learning-based model predictive control with Gaussian process models and stability guarantees," *Int. J. Robust Nonlinear Control*, vol. 31, no. 18, pp. 8785–8812, 2021. [Online]. Available: https://onlinelibrary.wiley.com/doi/abs/10.1002/rnc.5361

[16] M. L. A. M. Bloch, I. I. Hussein, and A. K. Sanyal, "Geometric structure-preserving optimal control of a rigid body," *J. Dynamical Control Syst.*, vol. 15, pp. 307–330, 2009.

[17] C. D. Santina, R. K. Katzschmann, A. Bicchi, and D. Rus, "Model-based dynamic feedback control of a planar soft robot: Trajectory tracking and interaction with the environment," *Int. J. Robot. Res.*, vol. 39, no. 4, pp. 490–513, 2020.

[18] Y. Kawano and K. Kashima, "An LMI framework for contraction-based nonlinear control design by derivatives of Gaussian process regression," *Automatica*, vol. 151, 2023, Art. no. 110928. [Online]. Available: https://www.sciencedirect.com/science/article/pii/S000510982300078X

[19] I. R. Manchester, J. Z. Tang, and J.-J. E. Slotine, "Unifying robot trajectory tracking with control contraction metrics," in *Robotics Research*. Cham, Switzerland: Springer, 2018, pp. 403–418, doi: 10.1007/978-3-319-60916-4_23.

[20] W. Wang and J.-J. E. Slotine, "On partial contraction analysis for coupled nonlinear oscillators," *Biol. Cybern.*, vol. 92, no. 1, pp. 38–53, 2005.

[21] G. Evangelisti and S. Hirche, "Physically consistent learning of conservative Lagrangian systems with Gaussian processes," in *Proc. IEEE 61st Conf. Decis. Control*, 2022, pp. 4078–4085.

[22] B. Paden and R. Panja, "Globally asymptotically stable 'PD +' controller for robot manipulators," *Int. J. Control*, vol. 47, no. 6, pp. 1697–1712, 1988, doi: 10.1080/00207178808906130.

[23] R. Ortega, A. Loría, P. J. Nicklasson, and H. Sira-Ramirez, *Passivity-based Control Euler-Lagrange Systems* (Communications and Control Engineering Series), 1st ed., London, U.K.: Springer, 1998.

[24] C. P. P. Herbert Goldstein and J. L. Safko, *Classical Mechanics*, 3rd ed., London, U.K.: Pearson, 2002.

[25] R. A. Layton, *Principles of Analytical System Dynamics*, 1st ed., New York, NY, USA: Springer, 1998.

[26] C. E. Rasmussen and C. K. I. Williams, *Gaussian Processes for Machine Learning*. Cambridge, MA, USA: MIT Press, 2006.

[27] M. Raissi, P. Perdikaris, and G. E. Karniadakis, "Inferring solutions of differential equations using noisy multi-fidelity data," *J. Comput. Phys.*, vol. 335, pp. 736–746, 2017.

[28] E. Solak, R. Murray-smith, W. Leithead, D. Leith, and C. Rasmussen, "Derivative observations in Gaussian process models of dynamic systems," in *Proc. Adv. Neural Inf. Process. Syst.*, 2002, pp. 1057–1064.

[29] M. A. Álvarez, L. Rosasco, and N. D. Lawrence, "Kernels for vector-valued functions: A review," *Foundations Trends Mach. Learn.*, vol. 4, no. 3, pp. 195–266, 2012.

[30] C. G. Albert and K. Rath, "Gaussian process regression for data fulfilling linear differential equations with localized sources," *Entropy*, vol. 22, no. 2, 2020, Art. no. 152.

[31] R. Dai, G. Evangelisti, and S. Hirche, "Physically consistent modeling & identification of nonlinear friction with dissipative Gaussian processes," in *Proc. 6th Annu. Learn. Dyn. & Control Conf.*, PMLR, vol. 2422024, pp. 1415–1426.

[32] M. Lutter, C. Ritter, and J. Peters, "Deep Lagrangian networks: Using physics as model prior for deep learning," in *Proc. Int. Conf. Learn. Representations*, 2019.

[33] R. M. Murray, Z. Li, and S. S. Sastry, *A Mathematical Introduction to Robotic Manipulation*. Boca Raton, FL, USA: CRC Press, 1994.

[34] A. R. Sudipto Banerjee, *Linear Algebra and Matrix Analysis for Statistics* (Texts in Statistical Science Series), 1st ed., Boca Raton, FL, USA: CRC Press, 2014.

[35] T. Ravichandran, D. Wang, and G. Heppler, "Stability and robustness of a class of nonlinear controllers for robot manipulators," in *Proc. Amer. Control Conf.*, 2004, pp. 5262–5267.

[36] C. Gumbsch, M. V. Butz, and G. Martius, "Sparsely changing latent states for prediction and planning in partially observable domains," in *Proc. Adv. Neural Inf. Process. Syst.*, 2021, pp. 17518–17531. [Online]. Available: https://openreview.net/forum?id=-VjKyYX-PI9

[37] R. Bhatia, *Matrix Analysis* (Graduate Texts in Mathematics Series) 1st ed., New York, NY, USA:Springer, 1997.

[38] S. Boyd and L. Vandenberghe, *Convex Optimization*, 7th ed. New York, NY, USA: Cambridge Univ. Press, 2004.

[39] W. Lohmiller and J.-J. E. Slotine, "On contraction analysis for non-linear systems," *Automatica*, vol. 34, no. 6, pp. 683–696, 1998.

[40] M. Corless, "Guaranteed rates of exponential convergence for uncertain systems," *J. Optim. Theory Appl.*, vol. 64, no. 3, pp. 481–494, 1990.

[41] E. F. Stephen Boyd, L. E. Ghaoui, and V. Balakrishnan, *Linear Matrix Inequalities System Control Theory*. Philadelphia, PA, USA: SIAM, vol. 15, 1994.

[42] J. R. Silvester, "Determinants of block matrices," *Math. Gazette*, vol. 84, no. 501, pp. 460–467, 2000. [Online]. Available: http://www.jstor.org/stable/3620776

Authorized licensed use limited to: TU Delft Library. Downloaded on July 10,2026 at 10:21:06 UTC from IEEE Xplore. Restrictions apply.

[43] C. Della Santina, R. K. Katzschmann, A. Biechi, and D. Rus, "Dynamic control of soft robots interacting with the environment," in *Proc. 2018 IEEE Int. Conf. Soft Robot. (RoboSoft)*, 2018, pp. 46–53.
[44] R. S. Penning and M. R. Zinn, "A combined modal-joint space control approach for continuum manipulators," *Adv. Robot.*, vol. 28, no. 16, pp. 1091–1108, 2014.
[45] R. Featherstone, *Rigid Body Dynamics Algorithms*, 1st ed. New York, NY, USA: Springer, 2014.
[46] D. Duvenaud, "Automatic model construction with Gaussian processes," 2014. [Online]. Available: https://www.repository.cam.ac.uk/handle/1810/247281



Giulio Evangelisti received the B.Sc., M.Sc., and Doctor of Engineering degrees in electrical engineering and information technology from the Technical University of Munich (TUM), Munich, Germany, in 2017, 2019, and 2025, respectively.

From 2017 to 2018, he was part of the Signal Generator Department, Measurement Technology Division, Rohde & Schwarz GmbH & Company KG, Munich, and from 2019 to 2020 a Full-time Control Engineer with Blickfeld GmbH, Munich. From 2021 to 2024, he was a Ph.D. candidate with the Chair of Information-Oriented Control, TUM School of Computation, Information and Technology. Since 2024, he has been with MTU Aero Engines AG in the predevelopment of flying fuel cell technologies for hydrogen-electric zero-emission aircraft propulsion systems. His research interests include the stability of data-driven control systems, physically consistent machine learning, robotics, nonlinear systems, and extremum seeking.



Cosimo Della Santina (Senior Member, IEEE) received the Ph.D. (cum laude) degree in robotics from the University of Pisa, Pisa, Italy, in 2019.

He was a Visiting Ph.D. Student and later a Postdoctoral Researcher with the Computer Science and Artificial Intelligence Laboratory, Massachusetts Institute of Technology, from 2017 to 2019. He was a Senior Postdoctoral with the Technical University of Munich, where he also was a Guest Lecturer. He is currently an Associate Professor with TU Delft, Delft, The Netherlands, and a Research Scientist with the German Aerospace Center (DLR), Munich, Germany. At TU Delft, he leads the Physical Intelligence (PhI) Lab, where his research focuses on endowing physical systems—particularly elastic and soft robots—with motor intelligence through co-design, modeling, control, and learning.

Dr. Della Santina was the recipient of several awards, including the euRobotics Georges Giralt Ph.D. Award in 2020, IEEE RAS Early Academic Career Award in 2023, NWO VENI Fellowship, and an ERC Starting Grant. He is a Principal Investigator in multiple European and Dutch research projects and the co-director of the Delft AI Lab SELF.



Sandra Hirche (Fellow, IEEE) received the Diploma Engineer degree in aeronautical and aerospace engineering from the Technical University Berlin, Berlin, Germany, in 2002, and the Doctor of Engineering degree in electrical and computer engineering from the Technische Universität München (TUM), Munich, Germany, in 2005.

She holds the TUM Liesel Beckmann Distinguished Professorship and heads the Chair of Information-oriented Control in the Faculty of Electrical and Computer Engineering, TUM, since 2013. From 2005 to 2007, she has been a PostDoc Fellow of the Japanese Society for the Promotion of Science, Fujita Laboratory, Tokyo Institute of Technology, Tokyo, Japan. Prior to her present appointment, she has been an Associate Professor with TUM. She has authored or coauthored more than 200 papers in international journals, books, and refereed conferences. Her main research interests include learning, cooperative, and distributed control with application in human–robot interaction, multirobot systems, and general robotics.

Authorized licensed use limited to: TU Delft Library. Downloaded on July 10,2026 at 10:21:06 UTC from IEEE Xplore. Restrictions apply.